EMBRYONIC FLUCTUATIONS AT MARTENSITIC PHASE TRANSFORMATION

Kazuhiro FUCHIZAKI

OSAKA UNIVERSITY
GRADUATE SCHOOL OF ENGINEERING SCIENCE
DEPARTMENT OF MATERIAL PHYSICS
TOYONAKA OSAKA

EMBRYONIC FLUCTUATIONS AT MARTENSITIC PHASE TRANSFORMATION

Kazuhiro FUCHIZAKI

Department of Material Physics
Faculty of Engineering Science
Osaka University

February 1989

SYNOPSIS

The 'precursor phenomena' associated with the martensitic phase transformation or more general first order phase transitions in solids are discussed based on the idea that the key mechansism of the phenomena is attributable to the locally excited long-lived triply stable fluctuations, which consist of 'embryos' of low temperature phase structure. We refer to those heterophase fluctuations as 'embryonic fluctuations'.

A new prescription to describe a general mechanism of the martensitic phase transformation in bcc-based alloys in the context of the embryonic fluctuation is presented. A 'three-state' spin variable which specifies local creation and annihilation of the embryo is defined, and the coupling of the spins to the lateral displacements of embryos is taken into account. An effective hamiltonian can be obtained in terms of the embryo creation energy and the interembryo interaction energy via phonons. Overall characteristics of the transformations including the precusor state are successfully explained by a semi-microscopic treatment based on the hamiltonian. Applications to real materials, in particular to the 7R-type martensite in NiAl, are discussed.

A Ginzburg-Landau free energy functional is then derived from the hamiltonian so as to discuss the precursor phenomena on a thermodynamic basis. Spatially modulated solutions of the order parameter as well as of strain field are obtained, which are identified as the macroscopic version of the embryonic

fluctuations. By utilizing the solutions diffraction patterns are calculated, which turn out to reproduce the observed anomalous diffraction effects at martensite transformation. Lastly an underlying significance of the physical meaning of the precursor phenomena will be emphasized.

CONTENTS

§ 1. INTRODUCTION

Structural phase transitions, occurring when a material changes its crystallographic structure, has long been one of the subjects for material scientists as well as for physicists. The earlier studies of these transitions were measurements of macroscopic properties such as specific heat, dielectric susceptibility, thermal expansion, etc., and were accelerated by the practical purpose of various applications of these materials; for example, the use of ferroelectrics as piezoelectric components and as pyroelectric detectors. There has also been a great deal of effort devoted to elucidating the nature of structural phase transitions at a more microscopic level and have succeeded to bring much understanding of structural phase transitions during late 50's and 70's - in a large part owing to the development of experimental techniques which enabled the microscopic properties to be probed with improved accuracy.

One of the outstanding findings was obtained from the investigations on materials having the distorted perovskite structure,[1] which showed that at least at some structural phase transitons the atoms in the distorted phase are slightly displaced away from the equilibrium positions of the high temperature phase, leading to the suggestions by Cochran[2] and Anderson[3] that these phase transitions might be the result of an instability of the crystal against a particular phonon mode of the high temperature phase. Since that suggestion, exhaustive investigations have been devoted to the so-called 'soft modes'[4]

associated with structural phase transitions and at least for these 'displacive' phase transitions their existence seemed to be well established in 70's.

There are other structural phase transitons where the phase transition is associated with an ordering of some variable which is disordered in the high temperature phase. A well known example of this behavior of 'order-disorder' type is the ferroelectric transition in $NaNO_2$ [5], in which above the transition temperature the N atoms of the triangular NO_2 groups are oriented either in the positive or the negative b axis with equal probability whereas below the transition temperature their orientations are aligned in either one of the two directions. Since the reorientational process of the NO_2 involves very large displacements (which far exceed the phonon amplitude), these motions cannot be described in terms of small displacements about the high temperature phase positions; In these order-disorder systems, 'soft mode' idea is less effective than in the displacive materials.

Nevertheless, the order parameters which characterize the phase transition can be described either by some of the phonon modes for the displacive type and by classical pseudospin modes to the order-disorder type. Just at the transition temperature the amplitude of the fluctuations of these modes diverge and frequency of particular phonon modes will soften in the former while in the latter critical slowing down toward equilibrium will be observed. These phenomena have attracted considerable

attention as 'critical phenomena'[6] at the second order phase transitons.

On the other hand, in some metals or alloys similar displacive transformations which we call in general 'martensite transformations'*1,[7] have long been known to exist. Early developments of the theory to this displacive transformations were the geometric description of the crystallographic orientation relationships[7] between martensite phases and the parent phase. Later, application of soft mode concept has been attempted, which has turned out to be quite ineffective. The origins and mechanisims of displacive behavior in these metals and alloys are still an area of considerable controversy.

However, recent experimental investigations have revealed various kinds of anomalous behavior above martensite transformation. The unusual properties observed above the transiton temperature are called 'precursor phenomena'.[8-22] As will be mentioned in some detail in the following section, the precursor phenomena have some similarity to the 'critical phenomena', but there seems to be an essential difference. The principal concern of this thesis is these precursor phenomena,

---

*1 The definition of martensitic transformation is somewhat ambiguous. In this thesis the term 'martensitic transformation' referes to all types of cooperative displacive transformations from single phase to single phase without accompanying any atomic diffusion.

because to clarify what happens just above the transition temperature is considered to be the key to open the door locked over fifty years.

The purpose of the present thesis is to elucidate the underlying microscopic (or semimicroscopic at least) mechanism leading to the martensite transformation, by which overall phase transformation scheme can be described in consistency with the experimental results in particular with the precursor phenomena.

This thesis is organized as follows; In §2, as the microscopic origin of the transformation, we introduce the idea of 'embryonic fluctuations'. The embryonic fluctuation is the coherent thermal fluctuations which simulate the low temperature structure locally and temporally. Various kinds of precursor phenomena are briefly discussed, in order to suggest qualitatively that the existence of the 'embryonic fluctuations' gives a consistent picture of the overall process of the martensite transformation.

Based on the idea of embryonic fluctuation, a new prescription to describe microscopic mechanism of the martensite transformation in bcc alloys is presented in §3. We define a 'three-state spin' variable which specifies local creation and annihilation of the 'embryo' of the low temperature phase, and take into account of the coupling of the spins to the lateral displacements of the embryo, thus greatly reducing the degrees of freedom of the whole system. We obtain an effective hamiltonian of the system given in terms of the embryo creation energy and the embryo-embryo interaction energy via phonons. The phase

transition scheme is investigated based upon the model hamiltonian. Applications to 9R martensite, which often appears as the low temperature structure of bcc-based alloys, and to so-called 7R martensite particulary observed in Ni-Al are presented. Precursor phenomena in Au-Cd are also analyzed on this model. Contained in the last subsection in §3 is the summary of our results and a comparison is made with another theory recently presented concerning the formation of 7R martensite. Possibility to include some finite temperature effect on our predicted ground state configuration for the martensite structure is discussed so as to explain the experimentally observed diffraction line shape. A task which has remained in our treatment to the complete understanding of the microscopic mechanism of the martensite transformation is also discussed.

In contrast to the semimicroscopic theory in §3, we develop in §4 the Ginzburg-Landau theory for the martensite transformation (or more generally for the first order phase transition in solids) to elucidate the relationship between the existence of the embryonic fluctuations and the precursor phenomena from a thermodynamic standpoint. We derive the coarse-grained free energy functional from the semimacroscopic spin hamiltonian used in §3. The coupling of the order parameter to a strain is then taken into account. The solution of the order parameter which minimizes the free energy above the transition temperature is given under suitable boundary conditions, which leads to the embryonic fluctuation. These results are utilized to calculate the diffraction pattern, which reproduces the

characteristics of observed diffraction effects discussed in §2. In summary and discussion we will present a comparison of the obtained results with recent experimental data. Also we will discuss the points beyond which our theory has proved to be inadequate, and the possible extension of our theory.

The last section is devoted to the conclusion, in which the significance of the physical meaning of the 'precursor phenomena' is addressed in contrast to the 'critical phenomena' at the second order phase transition.

§ 2. A SURVEY OF RECENT DEVELOPMENTS

2.1 An Introductory Remarks on Embryonic Fluctuations

Recent significant progress in understanding of the nature of martensite transformation in bcc-based metals has been based on the lattice instability against {110}<1$\bar{1}$0> shear strains,[23] which was pointed out forty years ago. Precursor phenomena, that often seem uniquely related to the ensuing symmetry changes, suggest that parent phases are effectively 'preparing themselves' for the transformations.

From investigations on the effective path to transformation, together with the consideration on the above lattice instability, Krumhansl[24] has claimed that, in contrast to the soft mode mechanisms based on charge density waves due to Fermi surface effects put forth by many authors, intrinsic bistable slow thermal fluctuations of the {110} planes in <1$\bar{1}$0> directions due to the extreme phonon anisotropy can just be the microscopic origin of the transformation.

Clapp, Guénin and Gobin[25] discussed the presence of stresses and strains around the impurities of the lattice which can enhance a local mechanical instability against {110} <1$\bar{1}$0> shear strains which gives rise to growth of 'locally soften microdomains'. Their treatment gives a possibility of the existence of microdomains of the low temperature phase induced around defects such as vacancies, interstitials above the transition temperature. A complete description along their lines

which is comparable with experimental data is still lacking however.

On the other hand, Mendelson[11] has proposed the soft mode lattice-variant-shear-theory which is based on the partialized dislocation model; The separation r of the partial dislocations, $\mathbf{b}_1$ and $\mathbf{b}_2$, is given in terms of the stacking fault energy γ_f as[26]

$$r = \frac{K}{2\pi\gamma_f} \mathbf{b}_1 \cdot \mathbf{b}_2 \qquad (2.1)$$

where K is the elastic energy factor for the faulting partial. As T comes close to T_c, γ_f decreased with the microdomain growing, and eventually at T_c, $\gamma_f = 0$ and the transformation dislocations will spread across the crystal and the transformation will be completed. Although the idea is clear, his explanation is still in a qualitative frame.

Yamada and co-workers[27] presented somewhat different picture which is called 'modulated lattice relaxation (MLR)' or 'dressed embryo' model. The MLR or the 'dressed embryo' is essentially a microdomain which simulates locally and temporally the low temperature structure. It is quite similar to the 'local soft mode' picture described above, but the difference is that they considered the dressed embryos are intrinsic fluctuations which will be thermally created without impurities.

In this thesis we refer to those microdomains as 'embryonic fluctuations'. We note, at this stage, that we consider those fluctuations are essentially triply stable (hereafter,

abbreviated as tristable) rather than bistable as claimed by Krumhansl[24] and others[25,28,29]; that is, the potential to which the order parameter is subjected should have triple minima having degenerate metastable states above T_c.

Based on the embryonic fluctuation picture, the process of transformation can be visualized generally as follows: At temperatures far above the transition temperature, embryos are frequently created by thermal excitation, but will soon be annihilated with a relaxation time $\tau_{emb} \sim e^{\Delta/k_B T}$, where Δ is an energy barrier height to form an embryo. Moreover, embryos will stay 'bare' because τ_{emb} is too short to induce the strain field around the embryos. As the temperature is lowered, so that the embryos become long lived in comparison with the propagation time of the elastic wave, they can be 'dressed', i.e., they can accompany the strain field around themselves. In the temperature range where embryo density is not still very high, the embryos are oriented randomly within equivalent directions satisfying cubic symmetry on average. This state may be identified to be the precursor state*2. As the temperature is further decreased, the creation energy of a embryo will be decreased. At the same time, a long-range indirect interaction between embryos via strain field around them develops which tends to orient the neighboring embryonic fluctuations ('dressed embryos') into the same direction, and eventually the whole lattice is cooperatively

---

*2 This state is often referred to as premartensite phase in metallurgical literature.

covered with the ordered embryos, which is nothing but the low temperature phase. The transition temperature is well-defined in view of cooperative nature of the process.

If this picture is correct, the martensitic transformation can be described by the 'key words' such as embryo creation energy, embryo-embryo interaction, equilibrium embryo density etc..

2.2 Precursor Phenomena

2.2.1 Diffraction Studies

Precursor phenomena which signal the transformation have been detected in various studies[9,10,12-20]; Scattering techniques including X-ray, electron and neutron scattering show; phonon dispersion curves with a dip at $\mathbf{q} = \mathbf{q}_0$ (a wave number characteristic to the low temperature structure, see Table I), satellite diffraction spots near but not exactly at $\mathbf{q}_0$, anomalous broadening of diffraction lines, the central peaks and tweed structures. Let us consider these anomalies in connection with the embryonic fluctuations.

a) Superlattice reflections appearing above T_c

Various kinds of diffraction experiments[17] have revealed that the diffraction patterns of bcc alloys exhibit superlattice (satellite) reflections even above the transformation

temperature. These reflections should appear in the martensite phase but should be absent in high temperature phase. One of the possible interpretations is that the symmetry of the system has already broken lacally while the overall lattice symmetry still maintains the original cubic symmetry on average. These results, therefore, strongly suggest that the embryos of the low temperature structure exist above T_c.

b) Anomalous incommensurability

As is mentioned in (a), the superlattice (satellite) reflections are already present above T_c as the precursor. In some cases, the position of superlattice reflections is not located exactly at commensurate positions $\mathbf{q}=\mathbf{q}_0$ but are slightly shifted from those positions.[18] Detailed X-ray diffraction studies[19,20] have revealed surprising peculiarities in this incommensurability. The anomaly is characterized by that the incommensurability changes depending on the reference Brillouin zone. This Brillouin zone-dependence of the shifts cannot be explained by any simple incommensurate structures consist of discommensurations with constant amplitude. Yamada et.al.[27] have shown by using lattice dynamical models that the possible microscopic origin to this anomalous incommensurability is due to the existence of the 'dressed embryos'. We will return to this phenomena in §4 and clarify from a different standpoint the close relationship between the anomalous incommensurability and the existence of the embryonic fluctuations.

c) The central peak in neutron spectra

According to the MLR picture the embryonic fluctuations can enlarge their correlations as T approaches to T_c with negligible activation. Following Mendelson,[11] let us estimate the lifetime τ_{emb} of a embryonic fluctuation just above T_c, where the dominant mechanism of the relaxation of the embryonic fluctuations may be due to the annihilation of domain boundaries separating the embryonic fluctuations from the matrix. Let us consider that at domain boundaries the transformation dislocations, whose density is typically $N_d \simeq 10^7$ cm^{-2} for annealed crystals, are localized. Assuming that the speed of travelling boundary V_d is about one-tenth of the speed of sound $V_s \simeq 3 \times 10^5$ cm/sec; $V_d \simeq 3 \times 10^4$cm/sec, then the average size of an embryonic fluctuation is $\ell = N_d^{-1/2} \simeq 3 \times 10^{-4}$ cm and the $\tau_{emb} = \ell/V_d \simeq 10^{-8}$ sec. This yields the lower limit for the value of τ_{emb} for given V_d, (because the assumption that all the dislocations are localized at the domain boundaries results in the lowest value for ℓ,) and is in fact in the range of the central peak scattering.[15] The intensity of the central peak increases rapidly as T approaches to T_c and, because of the cooperative nature of the domain growth, the energy for growth of the embryonic fluctuations will diminish rapidly, giving rise to a narrow energy width (small energy transfer) and slowing down, which is consistent with the late stage dynamics of transformation based on the MLR picture.

d) Tweed structures in TEM

A characteristic microstructure is often observed with TEM in the precursor state of many materials, which is referred to as 'tweed structure'.[10] Recently, Clapp et.al.[29] have obtained 'tweed' diffraction pattern by model calculations using molecular dynamics method. The tweed structure is considered to be the strain fringe due to the existence of the embryos of low temperature phase embedded in the matrix of high temperature phase.

2.2.2 Other Experimental Results

Since the exisitence of the quasistatic embryonic fluctuations modifies elastic, electric, and magnetic fields of the crystal, they can interact with applied fields to give rise to various anomalies of the physical properties. Other measurements[8] make use of the increased susceptibility of the crystal to applied fields which interact with the above correlated fluctuating fields associated with the embryonic fluctuations. Effects due to elastic softening consist of changes in the elastic constants, internal friction, pseudoelasticity, etc. Additional observations are made to show anomalies in specific heat and electric resistivity.

a) Pseudoelasticity and shape memory effect; Ferroelasticity

B2 type and some other alloys are highly susceptible to an elastic field, showing significant pseudoelasticity and shape

memory[30] due to the low energy structure*3 (§2.2.1 (c)) of phase boundaries separating embryonic fluctuations from the matrix above T_c and of self-accommodating phase boundaries separating different variants below T_c.[31] The presence of embryonic fluctuations above T_c determines its pseudoelasticity behavior for the applied stress while the degree of self-accommodation between variants defines the shape memory behavior for the temperature below T_c. These behaviors can easily be imagined from the cooperative MLR picture in connection with a simple (pseudo)spin system in a field conjugate to the spin.

b) Specific heat anomaly

Anomaly in specific heat[21,22] implies an increase in the number of degrees of freedom due to large scale embryonic fluctuations. These additional degrees of freedom include (i) fluctuating ionic shifts due to fluctuations of order parameter (i.e., embryonic fluctuations), (ii) increased fluctuations of the embryos as T approaches to T_c and their increased correlations, (iii) the onset of the habit plane shear on any of the four equivalent systems (plane group) in each of the six equivalnet variants (thus 24 possible variants arise), and (iv) divergence in the range of correlation between embryonic fluctuations and self-accommodation among the fluctuating variants.

---

*3 In fact these phase boundaries are given as 'solitons' which cost no energy with repect to the translation (see §4.3).

c) The anomaly in electric resistivity

A peak in electric resistivity[21,22] implies an increase in the number of degrees of freedom by which electrons are scattered, which is consistent with specific heat anomaly.

These anomalies (specific heat and electric resistivity anomalies) are often observed above T_c as if there is a new transition point to so-called premartensite phase.[22] However, the point at which these anomalies are found is largely dependent on crystallization condition. The exact mechanism which explain these anomalies satisfactorily is still not completely elucidated.

§ 3. A SEMI-MICROSCOPIC MODEL FOR MARTENSITIC PHASE TRANSFORMATION

In this section we will first introduce a general microscopic (or semimicroscopic) model which can describe the phase transformation with embryonic fluctuations in the precursor state. Two principal approximation schemes currently employed in microscopic theories are then presented; One is the independent site approximation and the other the independent mode approximation. We will suitably modify the general model to obtain a more reduced model for the description of the martensite transformation in question. The modification will be done in a sense of the independent site approximation that we shall retain explicitly the local variable. To obtain physical quantities we develop a mean field treatment to our model hamiltonian, because it is sufficient to qualitatively explain the currently available experimental results. The advantage of our approach is stressed by the comparison of the resultant low temperature structure of Ni-Al with that obtained by the different way based on, as one might say, rather the independent mode approximation scheme.

3.1 Definition of The Model

The simple model of which physical properties will be taken out is depicted in Fig.1, and is defined formally by the classical hamiltonian

$$H = T\{p\} + V\{u\} \tag{3.1}$$

with

$$T = \frac{1}{2} \sum_j p^2(j) \quad , \tag{3.2}$$

$$V = \sum_j V_{loc}(u(j)) + \frac{K}{2} \sum_{<j,j'>} (u(j)-u(j'))^2 \ . \tag{3.3}$$

Here the coordinate u(j) and p(j) denote, respectively, the displacements and momenta of a set of atoms, of unit mass, whose high temperature phase equilibrium positions (which lie in the central most stable minima of V_{loc}'s) with respect to which the displacements are defined consist of N sites of a d-dimensional hypercubic lattice of period a_0. The atoms are supposed to interact through a harmonic nearest neighbor coupling (the second term of eq.(3.3)) and to reside in a single particle potential V_{loc} with triply stable states. As is emphasized in §2.1, the fluctuations we shall treat are not, so to speak, inter-domain fluctuations associated with the widely used bistable (double-well) potential[32] but the heterophase fluctuations, in particular, in those temperature ranges where the high temperature phase is still stable. Moreover fluctuations with opposite displacement amplitude will allow to appear, reflecting the microtwin structure of the low temperature phase. In addition, the potential may be thought of as having a uniaxial anisotropy, which effectively restricts displacements to a single direction - hence the scalar character of the coordinates u(j)

and p(j). Keeping in mind these characteristics, we shall take this potential V_{loc} to have the simple form

$$V_{loc}(u) = \frac{a}{2} u^2 + \frac{b}{4} u^4 + \frac{c}{6} u^6 \qquad (a>0,\ b<0,\ c>0)\ . \qquad (3.4)$$

Here we allow for the coefficents a, b and c to be temperature-dependent, and in this sense our model is still semimicroscopic. Finally note that we consider a situation where an external field is absent. Including this effect is straightforward and we shall omit that influence for simplicity.

We will often find it more convenient to consider a Fourier representation of our system. The real space hamiltonian (3.1) through (3.4) is readily Fourier transformed into in the form

$$H = T\{P\} + V\{Q\} \qquad (3.5)$$

through

$$P(\mathbf{q}) = N^{-1} \sum_j p(j)\ e^{i\ \mathbf{q}\cdot\mathbf{R}(j)} \qquad (3.6)$$

$$Q(\mathbf{q}) = N^{-1} \sum_j u(j)\ e^{i\ \mathbf{q}\cdot\mathbf{R}(j)} \qquad (3.7)$$

with

$$T = \frac{N}{2} \sum_{\mathbf{q}} |P(\mathbf{q})|^2 \quad , \qquad (3.8)$$

$$V = \frac{N}{2} \sum_{\mathbf{q}} [\, a + 4dK\, J(\mathbf{q}) \,]\, |Q(\mathbf{q})|^2$$
$$+ \frac{Nb}{4} \sum_{\tau} \Big[\prod_{j=1}^{4} \sum_{\mathbf{q}_j} \Big] \prod_{j=1}^{4} Q(\mathbf{q}_j)\, \delta(\mathbf{q}_1+\mathbf{q}_2+\mathbf{q}_3+\mathbf{q}_4-\tau)$$
$$+ \frac{Nc}{6} \sum_{\tau} \Big[\prod_{j=1}^{6} \sum_{\mathbf{q}_j} \Big] \prod_{j=1}^{6} Q(\mathbf{q}_j)\, \delta(\mathbf{q}_1+ \cdots +\mathbf{q}_6-\tau) \ . \qquad (3.9)$$

Here the summations are carried out over wave vectors in the first Brillouin zone and τ denotes a reciprocal lattice vector. The Kronecker δ symbol reflects wave vector conservation and $J(\mathbf{q})$ is defined by

$$J(\mathbf{q}) = 1 - \frac{1}{d} \sum_{i=1}^{d} \cos(q_i a_0) \ . \qquad (3.10)$$

We will encounter such an expression in §4.1 on the way to a derivaiton of the coarse-grained free energy functional.

For the completeness of the general discussion we next outline briefly the two simplest schemes, by which theoretical treatments to the hamiltonian (3.1) or (3.5) can be developed, commonly referred to as 'mean field theory' and 'self-consistent phonon theory'. In fact each of the theories employs a 'mean field' character to reduce the many-body problem to a tractable single-body problem which is then solved 'self-consistently'. In the first of these schemes the intersite interaction is treated approximately while in the second of the schemes, it is the inter-mode interaction that is treated approximately. We shall, therefore, refer to the schemes as, respectively, the <u>independent site</u> and <u>independent mode</u> approximations.[32)]

3.2 The Independent-Site Approximation and The Independent-Mode Approximation

The essential character of the independent-site approximation is best revealed by considering the equation of motion, readily obtained from eq.s(3.1)-(3.4) as

$$-\ddot{u} = (a + 4dK)u(j) + bu^3(j) + cu^4(j) - 2K \sum_{j'}^{n\ n} u(j') \ . \tag{3.11}$$

The independent-site approximation replaces the last term in eq.(3.11) by

$$-2K \sum_{j'}^{n\ n} u(j') \simeq -2K \sum_{j'}^{n\ n} \langle u(j') \rangle^{IS} \equiv -4dKQ_0^{IS} \ , \tag{3.12}$$

the implicit assumption being that the evolution of each local coordinate is influenced only by the average of its interactions with the other coordinates. This scheme hence yields rather a good approximation to the system in which the interatomic interaction is long-ranged, for example, to a ferroelectrics[33] in which atomic displacements in a local potential produce dipoles. The superscript on the average indicates that it is to be calculated self-consistently in the indepedent-site ensemble implied by the approximation (3.12). The simultaneous set of equations (3.11) then decouple to give (hence we drop the subscript j) a set of N identical equations

$$-\ddot{u} = (a + 4dK)u(j) + bu^3(j) + cu^4(j) - 4dKQ_0^{IS} , \quad (3.13)$$

describing a single particle moving in the effective potential $\tilde{V}_{loc} = V_{loc}+2dKu^2$ under the influence of a mean field

$$E_{MF} = 4dKQ_0^{IS} . \quad (3.14)$$

The thermal average of the displacement of such a particle may be written as

$$Q_0^{IS} = \langle u \rangle^{IS}$$

$$= \int du\, u\, e^{-\beta(\tilde{V}_{loc} - E_{MF}u)} \Big/ \int du\, e^{-\beta(\tilde{V}_{loc} - E_{MF}u)} . \quad (3.15)$$

We have thus obtained self consistent-set of eq.s(3.13)-(3.15).

We next note the second major decoupling scheme - the independent-mode approximation. The assumption underlying the independent-mode ('self-consistent phonon'[34]) approximation, and their relationship to those of the independent-site approximation, are presented most clearly in terms of the equation of motion of the Fourier components, which follows from eq.s(3.5),(3.8) and (3.9) as

$$-\ddot{Q}(\mathbf{q}) = (a + 4dK\, J(\mathbf{q}))\, Q(\mathbf{q}) + b \sum_{\tau} \Big[\prod_{j=1}^{3} \sum_{\mathbf{q}_j} \Big] \prod_{j=1}^{3} Q(\mathbf{q}_j)\, \delta(\mathbf{q}_1+\mathbf{q}_2+\mathbf{q}_3-\mathbf{q}-\tau)$$

$$+ c \sum_{\tau} \Big[\prod_{j=1}^{5} \sum_{q_j} \Big] \prod_{j=1}^{5} Q(q_j)\ \delta(q_1+\cdots+q_5-q-\tau) \ . \qquad (3.16)$$

The independent-mode approximation replaces terms which are higher order than the quadratic term by quadratic-order terms using Wick's theorem;[35]

$$\begin{aligned} & b \sum_{\tau} \Big[\prod_{j=1}^{3} \sum_{q_j} \Big] \prod_{j=1}^{3} Q(q_j)\ \delta(q_1+q_2+q_3-q-\tau) \\ & \simeq b \Big\langle \sum_{\tau} \Big[\prod_{j=1}^{3} \sum_{q_j} \Big] \prod_{j=1}^{3} Q(q_j)\ \delta(q_1+q_2+q_3-q-\tau) \Big\rangle^{IM} \\ & \equiv 3bN\ [Q(q)-\langle Q(Q)\rangle^{IM}] \Big\langle \sum_{q_1} Q(q_1)Q(-q_1) \Big\rangle^{IM} , \qquad (3.17) \end{aligned}$$

etc. In effect the crucial approximation here also has a 'mean field' character, the simplifying assumption being that the evolution of each Fourier component is influenced only by the average of its interactions with the other coordinates. The superscripts indicate that the averages are to be evaluated, self-consistently, in the independent-mode ensemble implied by the approximation. In performing these averages one must allow explicitly for the nonvanishing expectation value of the coordinate Q(0) in the ordered phase. Thus we write

$$Q(q) \equiv \hat{Q}(q) + \langle Q(q)\rangle^{IM} \qquad (3.18)$$

and equating

$$\langle Q(\mathbf{q})\rangle^{IM} = Q(0)\delta(\mathbf{q}) \ , \qquad (3.19)$$

we have again closed set of equations for the Fourier components. Although these schemes may offer some insights into the critical dynamics of the model system, such as critical exponents and amplitudes, we shall not go too far in these subjects here.

3.3 A Model for Martensitic Transformation

We now try to adopt the general model (eq.s(3.1)-(3.4)), with a suitable modification, to the case of bcc(ß)-martensite phase transformation. To begin with, let us consider a microscopic process of the martensite transformation. To this end, first remember that the local lattice instability (or local lattice softening), which is mentioned in §2.1, can occur prior to the transformation. In a bcc(ß) lattice this instability arises along the <110> axes (see Table I). With the aid of this concept of local softening of TA phonon modes we can develop quite a new view to construct the martensite structure from a bcc(ß) lattice as follows;

(i) Start from the small amplitude phonon condensed state with $\mathbf{q} = \mathbf{q}_0$ (see Fig.2(a)) along one of <110>-directions, for example, in the [110]-direction, $\mathbf{q}_0$ being the dip position in the phonon dispersion.

(ii) Produce local fcc structure composed of several successive layers by increasing the amplitude of the condensed

phonon and/or distoring the shape of the wave (or introducing higher order harmonic waves) (Fig.2 (b)). The parent lattice thus simulates or prepares locally the low temperature structure. We often refer to this local fcc structure as a 'cluster', which is nothing but an 'embryo' of the low temperature phase.

(iii) Introducing an appropriate amount of slip at the cluster boundaries between the local fcc structures along $[1\bar{1}0]$-direction in order to relax the local stress (Fig.2(b)). Notice the relative atomic configuration at the cluster boundaries in Fig.2(b) is definitely unstable.

These procedures (i) through (iii) result in the martensite structure (Fig.2(c)). In fact the above prescription will be applied to real systems in §3.5.

Note that, besides the local lattice instability, this view is based on the assumption that the system has the tendency to form locally the fcc type (ABC-type) stacking along the [110]-direction, composed of at least three successive basal (110) planes*4, which acts as the embryo.

With this view we then formulate the model hamiltonian, which will turn out to belong to the class expressed by eq.s(3.1)-(3.4). If we consider, in general, that the 'cluster' is the smallest unit with physical meaning associated with the

---

*4 At the same time, elongation and contraction along the other two axes normal to the [110]-direction occur, which construct the hexagonal basal plane. Since this deformation is irrelevant for the later discussion, we just neglect this deformation hereafter.

phase transition mechanism, the degree of the freedom of motion of the whole system under consideration can be simply reduced to the degree of freedom concerning the clusters; the translation of the center of mass of the cluster along $[1\bar{1}0]$ and the shear deformation or the 'tilt' of the cluster.

The first point to make is that there are two equivalent tilted states (see Fig.3). Thus, together with the undeformed state, the state of the cluster can be represented by a 'spin' variable with three eigenstates; $\sigma = (1,0,-1)$, among which $\sigma=\pm1$ are energetically degenerate by the symmetry of the parent bcc phase*5.

In order to describe appropriately the strain energy stored at the cluster boundaries, both ends facing each other of the two consecutive clusters are connected by harmonic springs with spring constant κ (see Fig.4(a)). The local potential-spring picture which corresponds to the microscopic state shown in Fig.4(a) is depicted in Fig.4(b) in order to stress the physical equivalence of our specific model for the martensite transformation to the general model (eq.s(3.1)-(3.4)). However, we make up, to our end, a more tractable hamiltonian than that exressed by eq.s(3.1)-(3.4). A modification is made such that, as was introduced the discretized variable σ, there is the

---

*5 The degeneracy refers to that for the states with a fixed $\mathbf{q}_0$. Since there are six equivalent <110> orientations, the total degeneracy of the tilted cluster should be twelve in the real cubic system.

contribution of creation energy ε associated with the local formation of the tilted cluster state, which is originated from the local potential energy V_{loc} of the cluster. As is shown in Fig.4(b), we are considering that the each minimum of the local potential corresponds to the states σ = 1, 0, or -1;

$$V_{loc}(u) \rightarrow \varepsilon\sigma^2 \tag{3.20}$$

The creation energy ε corresponds to the energy difference between σ = 0 and σ = ±1. To include the strain energy contribution, let u_j be the lateral displacement (slip) of the j-th cluster relative to (j-1)-th cluster. Furthermore, let u_j be equal to zero when two consecutive clusters are in high temperature structure position. The energy associated with the cluster configuration can then be written as

$$U\{\sigma_j,u_j\} = \sum_j \frac{\kappa}{2} u_j^2 - \alpha u_j(\sigma_{j-1} + \sigma_j) \ , \ \alpha > 0 \ , \tag{3.21}$$

where the first term is simply an elastic energy. Note that in the second term the coefficient α represents the effect of coupling between $\{\sigma_j\}$ and $\{u_j\}$. The ground state configuration for this interaction energy is readily seen to be σ_j=-1, u_j=-2α/κ or σ_j=1, u_j=2α/κ for all j. Together with (3.20), our microscopic hamiltonian is of the form;

$$H\{\sigma_j,u_j\} = \sum_j \varepsilon \sigma_j^2 + U\{\sigma_j,u_j\} \ . \tag{3.22}$$

Thus the cluster system is now expressed effectively by a (three-state) spin-phonon coupled system. The effects of the displacement field are readily renormalized through

$$e^{-\beta \tilde{H}\{\sigma_j\}} = \int d\{u_j\}\, e^{-\beta H\{\sigma_j, u_j\}} \tag{3.23}$$

to give an effective hamiltonian $\tilde{H}\{\sigma_j\}$ of the spin system. $\tilde{H}\{\sigma_j\}$ thus obtained is, apart from a trivial part,

$$\tilde{H}\{\sigma_j\} = \sum_j \tilde{\varepsilon}\, \sigma_j^2 - \tilde{J}\, \sigma_j\, \sigma_{j-1} , \tag{3.24}$$

where $\tilde{\varepsilon}$ and $\tilde{J}$ are the renormalized creation energy and the renormalized nearest neighbor interaction between spins (embryos) respectively, and are given by

$$\tilde{\varepsilon} = \varepsilon - \alpha^2/\kappa , \tag{3.25}$$

$$\tilde{J} = \alpha^2/\kappa \quad . \tag{3.26}$$

It should be noted that we are actually treating the ordering problem in three-dimensional space. In the final expression (3.24) σ_j means not a state of particular cluster in 1-D cluster chain but an averaged quantity with respect to all spins in a plane which contains j-th cluster and is normal to the wave vector $\mathbf{q}_0$. Thus the parameters such as ε, α and κ are not strictly of microscopic origin, but are semimicroscopic in the

sense that they are associated with statistical average within the layer.

3.4 Phase Transition Scheme

In order to discuss the phase transition from the high temperature bcc(β) phase, passing through premaretensitic state, to the low temperature martensite phase, we utilize the hamiltonian obtained in the previous subsection. The relevant quantities which we are concerned are the cluster order parameter $\langle\sigma\rangle$, and the average amount of slip of a cluster $\langle u\rangle$. In addition, the quantity $\langle\sigma^2\rangle$ is of special interest here, because this quantity corresponds to the equilibrium embryo density which can be experimentally detected by quasielastic neutron scattering or diffuse X-ray scattering. In fact Noda et.al.[20] have observed stong X-ray diffuse scattering in premartensitic region in Au-Cd, and inferred that the low temperature embryos may exist with high density even above the transition temperature.

Before calculating the above quantities some attention must be paid to the temperature dependences of the parameters in the hamiltonian. As is mentioned in §2.2, phonons belonging to [110]TA branch are weakly softened so that the spring constant κ may have a temperature dependence as $\kappa = \kappa_0(T-T_0)$ where T_0 is a fictitious critical temperature of intrinsic stability limit of the cubic phase which is considered to be far lower than the transition temperature. The creation energy ε of a single cluster

can also be temperature dependent since we interprete ε as a semimicroscopic quantity. Going back to the local potential as depicted in Fig.4(b), it would be quite reasonable to consider that ε is increasing with increasing temperature in order to be consistent with T-dependence of κ, because κ is associated with the curvature of V_{loc} at $\sigma = 0$, while ε is the energy difference of the minima of the same potential function. If this temperature dependence is given in a form of λT^{δ}, one can readily see that, from the eq.(3.29) below, $\delta > 1$ will be required because $<\sigma^2>$ must vanish at temperatures far above the transition temperature. The precise choice of δ is, however, inessential for the equilibrium behaviors of $<\sigma>$, $<u>$ and also $<\sigma^2>$ in the temperature region of interest. In fact, qualitatively the same results follow in our mean field treatment for $\delta > 1$. Here we have put $\delta = 2$ rather arbitrarily.

To proceed, we use the mean field approximation. Following the standard procedure, we have

$$< \sigma > = \frac{2 \sinh \beta z\tilde{J}<\sigma>}{2 \cosh \beta z\tilde{J}<\sigma> + \exp(\beta\tilde{\varepsilon})} , \qquad (3.27)$$

$$< u > = \frac{2 \alpha}{\kappa} < \sigma > , \qquad (3.28)$$

and

$$< \sigma^2 > = \frac{2 \cosh \beta z\tilde{J}<\sigma>}{2 \cosh \beta z\tilde{J}<\sigma> + \exp(\beta\tilde{\varepsilon})} , \qquad (3.29)$$

where z is the coordination number which is equal to 2 in our (pseudo) 1-D system. We introduce a dimensionless temperature $\tau = \lambda T/k_B$ and a dimensionless parameter $\Upsilon = \lambda^2\alpha^2/\kappa_0 k_B^3$. One of typical results, together with the corresponding experimental result for Au-Cd,[20] are shown in Fig.5 for the case of $\Upsilon = 20$. Here we have put $T_0 = 0$ for simplicity. For this value of Υ the first order transition occurrs at $\tau_c = 3.389$. Below τ_c the system exhibits cooperative ordering characterized by a non-zero value of $\langle\sigma\rangle$ and $\langle u\rangle$, which means that the martensite phase with the appropriate structure is stabilized below τ_c.

As is seen from eq.(3.28), $\langle u\rangle$ will tend to diverge as the temperature approaches to T_0. This has resulted by the assumption of complete harmonicity of the springs which link spins (clusters) together. In real systems this intercluster interaction must have strong nonlinearity for such a large displacement that exceeds the amplitude of phonons, and at temperatures below τ_c this nonlinearity is considered to be responsible for the lock-in of $\langle u\rangle$ to some value u_0

In Fig.5, it is noticeable that even above τ_c, where the system retains cubic symmetry, $\langle\sigma^2\rangle$ remains finite and slowly decays with increasing temperature as

$$\langle \sigma^2 \rangle \propto e^{-\tau + \Upsilon/\tau^2} . \qquad (3.30)$$

This feature is particulary important, because $\langle\sigma^2\rangle$ is proportional to the embryo density. The above feature justifies that under proper circumstances, there exists the equilibrium

state where the low temperature microstructures are distributed randomly with considerably high density before the phase transition takes place. This temperature region, therefore, just corresponds to the precursor (premartensitic) state. The hamiltonian (3.24) thus satisfactorily describe the transition nature between bcc phase and the martensite phase including the presence of precursor phenomena.

3.5 Application to Real Materials

We look into how our prescription for the transformation process mentioned in §3.3 works well to the real materials; The shape of the cluster (embryo) and the amount of slip of the cluster will actually be considered. We take up as examples two important cases; one is the formation of 9R martensite structure often observed and the other that of 7R-type martensite sturcture as a practically important case.

3.5.1 Application to 9R Martensite

To begin with, we apply our view to the bcc(β)-9R transition, since most of bcc-martensite transformations belong to this class and the situation is simple enough to elucidate our idea.

The 9R structure is well established and considered to be deduced from the following two successive processes;[36)]

(i) The symmetry change takes place due to small lattice distortion caused by a TA phonon mode condensation with the wave vector $\mathbf{q}_0$ = 1/3[110].

(ii) The distorted lattice is then deformed into the 9R type by introducing a macroscopic deformation, which is composed of the inclination of [110] axis (Bain strain) and the elongation and contraction along the other two axes perpendicular to [110] axis to construct (pseudo)hexagonal basal plane (see footnote 4).

An alternative view to construct 9R structure can be developed as follows (the general prescription mentioned in §3.3 should also be referred to.);

(i) TA phonon with $\mathbf{q}_0$=1/3[110] is locally softened (Fig.6(a)).

(ii) Local fcc structure (Cluster) of three succssesive layers is then produced bfurther increasing the amplitude of the condensed phonon (Fig.6(b)). This cluster is just the embryo of the 9R martensite.

(iii) The boundary slips along $[1\bar{1}0]$-direction are finally introduced in order to relax the local stress (Fig.6(b)), which in fact result in the 9R structure (Fig.6(c)). Notice that the (110) basal planes are now stacked as ABABCBCAC$\cdots$.

Apart from the specific case of 9R, when the system is unstable against a phonon mode with $\mathbf{q}=\mathbf{q}_0$ along [110]-direction, the same view holds if the size of the embryo is taken appropriately. For later convenience, we describe the postulated

shape of the embryo of the case for q_0=1/7[110] in Fig.7. The embryo shown in Fig.7(b) comes into play in the bcc(β)-7R type martensite transformation, which will be mentioned in the following.

3.5.2 Application to 7R Martensite

The low temperature phase of Ni-Al is of special interest, because Ni-Al undergoes martensitic transformation[37] from high temperature β phase to a particular 7R type structure. Extensive experimental studies show that this alloy has also the common features of martensitic transformations mentioned in §2.2. In fact phonon dispersion curves for the [110] $<1\bar{1}0>$ TA_2 branch in Ni_xAl_{1-x} reveal a pronounced minimum at q ~ 0.13 (x=0.63),[14] whose position in the q-space has concentration dependence, and substantial quasielastic scattering appears above the transition temperature. The intensity of the satellite reflections increases with decreasing temperature, and around T ~ 253K the crystal transforms to a martensite phase with a monoclinic unit cell.

Martynov et.al.[38] studied the structure of martensite phase by X-ray diffraction and proposed a specific structure model characterized by so-called (5 - $\bar{2}$) stacking of successive hexagonal layers(7R structure). Recently Shapiro et.al.[39] performed detailed neutron diffraction measurements. They studied intensity profiles of the satellite peaks and reconfirmed presence of superlattice reflections which are consistent with

the 7R structure, except that the peak positions shift slightly from the commensurate positions of exact 7R periodicity. Schryvers et.al.[40] also observed directly (5 - $\bar{2}$) type stacking by electron microscopy. It would be an interesting challenge to apply our model to this particular system.

Following our prescription, one can construct the structrue of the low temperature (ordered) phase as follows; (i) Consider the small amplitude TA phonon condensed state with q_0=1/7[110]. (ii) Simulate locally the fcc structure by increasing the amplitude and deforming the shape of the wave (Fig.8(a)). In this case the embryo or the tilted cluster should be composed of 6 layers as has been postulated in Fig.7(b). (iii) Introduce the boundary slips between the neighboring clusters (Fig.8(b),(c)). As is illustrated in Fig.8(c´), this procedure in fact construct qualitatively the (5-$\bar{2}$) structure. Notice that the resultant structure may be viewed as composed of alternating stacking of 6-layer fcc slab and 3-layer distorted bcc slab.

To be more quantitative, we allow the tilt angle θ of the fcc cluster to deviate slightly from the exact value to form the ideal fcc stacking (θ = 71.57 °). This is related to the fact that in Ni-Al, the basal plane does not show complete hexagonality in the martensite phase[*6]. An alternative reason for this incomplete fcc stacking may be ascribed to the incommensurability between the wave length of the soft phonon q_0=1/7[110] and the period of fcc stacking. Note that in the 9R martensite both periods are commensurate and complete fcc cluster is then formed. In this context, our model structure may be

expressed more exactly by the alternative stacking of (6-layer distorted fcc) - (3-layer distorted bcc). In the following analysis, we leave both the amount of slip u_0 and the tilt angle θ as parameters.

We now try to adjust the parameters so as to obtain agreements with the experimental data. From the observed monoclinic angle, the value of u_0 is determined to be $u_0 = 0.250$. The tilt angle is then determined within a relevant range of θ ($71.57^\circ \leqq \theta \leqq 90^\circ$) so that the relative intensity of superlattice reflections is fitted to the observed profiles by neutron diffraction measurement. By taking $\theta = 81.34^\circ$, we obtained fairly od agreement along $[2+\bar{\xi}\ 2+\xi\ 0]$ line. The profile is given in Fig.9. The obtained angle $\theta = 81.34^\circ$ is nearly equal to the corresponding angle $\theta = 80.54^\circ$ of the $(5\text{-}\bar{2})$ structure. The embryo of 7R martensite is thus considered to be freezed-in on the way to the complete fcc stacking.

As far as the relative intensity is concerned the results seem to be satisfactory. However, as stated above, the peak positions of experimental data are shifted from the commensurate position. This deviation apparently has no regularity both in

---

*6 According to the paper by Shapiro et.al. (Ref.39), the ratio γ of the principal axes a_m/b_m in the monoclinic a-b plane (pseudohexagonal basal plane) is given by $\gamma=1.54$. This value is just in between the ideal value for bcc lattice ($\gamma=\sqrt{2}$) and for fcc lattice ($\gamma=\sqrt{3}$). The observed monoclinic angle β_m is given as 94.37°.

magnitude and in direction. At the present stage, we are not able to give strict theoretical basis of the shift pattern.

However, notice that we have considered the fully ordered ground state configuration by taking $<\sigma>=1$. It would be quite possible that, at finite temperatures, the positions of embryos, and whence the positions of slips are more or less randomly distributed along the [110]-direction. This random configuration of embryos and slips may be the origin of Hendricks-Teller type irregurality[41] of the diffraction pattern, which will be briefly touched upon in §3.6.2.

3.6 Summary and Discussion

3.6.1 Summary of Results and Comparison wi Other Theories

We summarize the results obtained in this section as follows;

(i) We focus our attention upon the thermally induced embryos, which are considered to play an essential role in the martensitic transformation, and retain the degrees of freedom concerning the embryo motion by introducing a three-state spin variable σ. This leads to an effective hamiltonian composed of two parts; the one stands for the creation energy of embryos and the other the interaction energy between embryos via phonons.

(ii) Using the hamiltonian, the phase transition scheme is investigated with the mean field approximation to obtain the

embryo order parameter $\langle\sigma\rangle$, the average amount of slip $\langle u\rangle$, and the equilibrium embryo density $\langle\sigma^2\rangle$. With a suitable choice of the parameters, a first order transition takes place. Below the transition temperature, $\langle\sigma\rangle$ as well as $\langle u\rangle$ shows cooperative ordering, which correctly gives the martensite structre. On the other hand, $\langle\sigma^2\rangle$ is found to remain finite even above the transition temperature. This feature justifies the existence of the equilibrium state where the microstructures (embryos) of the low temperature phase are distributed randomly within the parent phase, which is noting but the so-called premartemsitic phase.

(iii) We applied our model to interprete the low temperature structure of Ni-Al. The so-called $(5\text{-}\bar{2})$ structure is reproduced as the 'ordered state' with respect to σ and u. Qualitative agreements of the calculated intensity profile based on this model structure and the experimentally observ neutron intensity spectra are obtained.

In spite of the simplicity, our model seems to be able to explain primary features of the martensite transformation including premartensitic behavior. Other theories mentioned in §2.1 have not, although the importance of the concept of 'embryo' or 'embryonic fluctuation' is recognized, yet been reached to the stage of a comparison with experimental results.

On the other hand, Gooding and Krumhansl[42] have treated the bcc-9R transition in Li from a different standpoint, in which the discussion is based upon the phenomenological Landau theory. The difference between theirs and ours is quite clear in the following sense; We take up independent-site scheme to retain

local variable σ_j while they prefer the independent-mode scheme to the order parameter ψ. In their free energy expansion, the uniform strain field e couples to the primary order parameter $\psi = A\, e^{i\,(\mathbf{q}_0 \cdot \mathbf{r} + \phi)}$ ($\mathbf{q}_0 = 1/3[110]$, $\mathbf{e} \,//\, [1\bar{1}0]$) in the form $e\psi^3$. Much attention is paid to the ground state solutions which minimize the free energy and to the dain-wall structure when the Ginzburg-like term for the order parameter is included.

Recently, they[43] have further extended the above theory to Ni-Al case. They specify the two independent order parameters; $\psi_1 = A_1\, e^{i\,(\mathbf{q}_0 \cdot \mathbf{r} + \phi_1)}$ and $\psi_2 = A_2\, e^{i\,(2\mathbf{q}_0 \cdot \mathbf{r} + \phi_2)}$, among which ψ_2 is <u>not</u> associated with any soft mode. The coupling to the uniform strain can then be described by the term $e\psi_1^2\psi_2^*$. They have obtained parameters to be fitted to the observed macroscopic strains. However, the values of A_1 and A_2 which should determine the relative displacement of each layer are left undetermined.

As far as the low temperature structure is concerned, there would be no essential difference between the results obtained by Gooding-Krumhansl's treatments and the present 'embryo ordering' picture. The difference is primarily seen in the premartensite phase. In the present treatment, the local variable σ_j is explicitly introduced. Hence, it seems to have the advantage to describe more naturally the pretransitional state in which the local symmetry has been already broken while the overall cubic symmetry is still retained.

3.6.2 Finite Temperature Effect: Hendricks-Teller Type Satellite Line Shape

We give some remarks on the low temperature structure of Ni-Al. As is mentioned in §3.5.2 we regard the amount of slip u_0 and the tilt angle θ as parameters, the former is determined by the observed monoclinic angle while the latter by comparing the calculated intensities with the experimental results in such a parameter range that $71.57^\circ \leqq \theta \leqq 90^\circ$. The $(5\text{-}\bar{2})$ structure is then almost uniquely determined in this parameter range. However it is necessary for the complete understanding of the structure to investiga satellite peak intesity profile in many Brillouin zones. Once again we emphasize that we refer just to the ground state configuration. Notice our standpoint is that the ground state configuration results from the cooperating effect between embryos formed by <u>local</u> deformation or distortion. Hence it is rather likely that the system includes stacking faults (deformation and growth faults) at finite temperatures. The analyses performed by Berliner and Werner[44] will therefore be needed to explain precisely the experimentally observed diffraction patterns.

3.6.3 Open Questions

Returning to our model hamiltonian, let us make some comments on our treatment. We have considered the ordering

problem in one-dimensional space along a particular [110] axis by averaging out all fluctuations normal to this axis. As is pointed out in footnote 5, there are six equivalent <110> orientations, and there is no particular reason to regard a single [110] direction as a special one. In real materials, embryos should be oriented randomly in all equivalent directions. In fact, anomalous shift pattern of satellite peaks observed in Ni-Ti-Fe and Au-Cd (see §2.2.1) are successfully explained[27] by introducing embryos having two different orientations. Allowing the six possible <110> orientations, the pseudospins should have the 12-fold degenerate excited states. We conjecture however that this will not cause any qualitative difference in the phase transition scheme described in §3.4.

Our hamiltonian is still semimicroscopic in the sense that ad hoc temperature-dependence of the embryo creation energy has been assumed. More microscopic basis is needed to understand the properties of the local potential V_{loc}. In addition, anharmonicity for e displacement field must be taken into consideration to suppress the unphysical divergence as has been mentioned in §3.4.

§ 4. THERMODYNAMICAL TREATMENTS FOR EMBRYONIC FLUCTUATIONS

In the preceeding section, we have developed a semi-microscopic theory based on the spin hamiltonian. One of the important results of the treatment is that the embryo density above the first order transition point have been calculated. Since $\langle\sigma\rangle=0$ in this temperature region, the system still maintains the symmetry of the high temperature phase on average. The situation $\langle\sigma^2\rangle\neq0$, while $\langle\sigma\rangle=0$, would mean that the symmetry of the system has been locally broken. The local symmetry breaking above the transition point should be one of the most important features of the embryonic fluctuation picture.

There is in fact clear experimental evidence of local symmetry breaking above the transition point: As was discussed in §2, the X-ray diffraction patterns often exhibit extra(satellite) reflections while the fundamental Bragg reflections still keeping the (high temperature) cubic symmetry. Moreover, the satellite reflections sometimes show anomalous incommensurability, that is the amount of incommensurability $\Delta\mathbf{q}$ is dependent on the reference Brillouin zone. It is challenging to apply the embryonic fluctuation model to understand these anomalous diffraction phenomena.

In order to achieve this end, we proceed as follows; instead of utilizing the microscopic hamiltonian directly, we first derive Ginzburg-Landau free energy density from the hamiltonian (3.24). Then a free energy functional which describes the first order phase transition including the coupling between the order

parameter and a macroscopic strain is established. An embryonic fluctuation naturally appears as a solution which minimizes the free energy above the transition temperature. It is straightforward to use the obtained solution of embryonic fluctuation to calculate the diffraction patterns.

The reason we first establish the free energy functional is that once the explicit expression of the free energy is given, the arguments can be based on purely phenomenologial standpoint. Hence the obtained results can give general perspective view of the origin of the local symmetry breaking.

4.1 Derivation of A Coarse Grained Free Energy

The order parameter associated with a displacive phase transition is the amplitude ξ of the particular phonon mode which freezes in the ordered phase. That is, the displacement in the low temperature (ordered) phase at the j-th site is given by

$$\mathbf{u}(\mathbf{r}_j) = \xi\, \mathbf{e}(\mathbf{q}_0)\, \exp(i\, \mathbf{q} \cdot \mathbf{r}_j) + \text{c.c.}\,, \qquad (4.1)$$

where $\mathbf{q}_0$ and $\mathbf{e}(\mathbf{q}_0)$ denote the wave vector and the poralization vector of the freezing (soft) mode respectively. For simplicity, let us assume that $\mathbf{q}_0$ is at the zone boundary along the direction of one of the principal axes, $\mathbf{a}$, of the crystal;

$$\mathbf{q}_0 = 1/2\ \mathbf{a}^*\,, \quad (\ |\mathbf{a}^*| = 2\pi / a\ ) \qquad (4.2)$$

and $\mathbf{e}(\mathbf{q}_0)$ is perpendicular to $\mathbf{a}^*$ (transverse mode). That is, the ordered structure is of antiferro-type.

As the starting point, let us calculate from the spin hamiltonian (3.24) the mean field free energy $F[<\sigma_i>]$ near the transition point T_c to generate a Ginzburg-Landau functional[45] as a function of the order parameter ξ. When an external field h_{ex} is involved in the hamiltonian (3.24), the mean field equation for $<\sigma_i>$, the average spin at site i, is given by (cf. (3.27))

$$<\sigma_i> = \frac{2 \sinh \frac{h_i + h_{ex}}{k_B T}}{e^{\tilde{\varepsilon} / k_B T} + 2 \cosh \frac{h_i + h_{ex}}{k_B T}} \quad , \tag{4.3}$$

where h_i is the mean field

$$h_i = \sum_j^{n\,n} \tilde{J} <\sigma_j> \quad . \tag{4.4}$$

The free energy $F[<\sigma_i>]$ should be related to h_{ex} by the following equilibrium condition

$$- \frac{\delta F}{\delta <\sigma_i>} + h_{ex}(<\sigma_i>) = 0 \, . \tag{4.5}$$

Solving eq.(4.3) explicitly with respect to h_{ex},

$$h_{ex}(<\sigma_i>) = - \sum_j^{n\,n} \tilde{J} <\sigma_j> + \frac{1}{\beta} \tanh^{-1} g(<\sigma_i>) \quad , \tag{4.6}$$

with

$$g(\sigma) = \frac{\sigma e^{\beta\tilde{\varepsilon}} + \sigma\sqrt{(\sigma^2 e^{\beta\tilde{\varepsilon}} + 4(1-\sigma^2))}}{\sigma^2 e^{\beta\tilde{\varepsilon}} + \sqrt{(\sigma^2 e^{\beta\tilde{\varepsilon}} + 4(1-\sigma^2))}} . \qquad (4.7)$$

From eq.(4.5) the free energy becomes (apart from a constant)

$$F[<\sigma_i>] = -\frac{1}{2}\sum_{<ij>}\tilde{J}<\sigma_i><\sigma_j> + \frac{1}{\beta}\sum_i \int_0^{<\sigma_i>} d\sigma \tanh^{-1}g(\sigma) . \qquad (4.8)$$

In fact minimization of eq.(4.8) with respect to $<\sigma_i>$ yields the mean field equation (3.27), as it should. Since we are considering a situation near T_c, we can expand $\tanh^{-1}g(\sigma)$ in power series of σ. Note here that since $\tanh^{-1}g(\sigma)$ is an odd function of σ, only odd powers appear upon expanded;

$$\tanh^{-1}g(\sigma) = \tilde{g}_1\sigma + \tilde{g}_3\sigma^3 + \tilde{g}_5\sigma^5 + O(\sigma^7) . \qquad (4.9)$$

When the expansion coefficients are actually calculated, one can see that the leading term in $\tilde{g}_3$ is negative while $\tilde{g}_5$ is positve definite on $T > 0$. We must, therefore, keep up to 5-th order in σ in the expansion so as to avoid the unphysical instability. Then introducing the Fourier transform σ_q through (cf. (3.7))

$$\sigma_q = N^{-1}\sum_j <\sigma_j> e^{iqj} , \qquad (4.10)$$

we find (cf. (3.9))

$$F[\ \sigma_q\ ]/N = -\frac{1}{2}\sum_q \left(2\tilde{J}(1-\frac{1}{2}q^2) - \frac{\tilde{g}_1}{\beta} \right) |\ \sigma_q\ |^2$$
$$+ \frac{\tilde{g}_3}{4\beta}\left[\prod_{j=1}^{4}\sum_{q_j}\right]\left[\prod_{j=1}^{4}\sigma_{q_j}\right]\delta(q_1+q_2+q_3+q_4)$$
$$+ \frac{\tilde{g}_5}{6\beta}\left[\prod_{j=1}^{6}\sum_{q_j}\right]\left[\prod_{j=1}^{6}\sigma_{q_j}\right]\delta(q_1+\cdots+q_6)\ . \qquad (4.11)$$

Here we keep only long wave length fluctuations in σ_q and, hence, in

$$\tilde{J}_q \equiv \sum_j^{n\ n} \tilde{J}\ e^{iqj} = 2\tilde{J}\cos q \qquad (4.12)$$

terms up to $O(q^2)$ have been kept. Through such a coarse graining procedure the continuous order parameter ξ is defined from eq.(4.10) as

$$\xi(x) = \frac{L}{2\pi}\int dq\ \sigma_q\ e^{iqx}\ , \qquad (4.13)$$

where L is the system size. (Note that $\xi(x)$ inherits a pseudo 1-D character of the spatial modulation of σ_i.) By using eq.(4.13), eq.(4.11) can be retransformed into

$$F[\xi] = \int dx\ \left[\ \frac{\tilde{J}}{2}(\partial_x\xi)^2 + \frac{a}{2}\xi^2 + \frac{b}{4}\xi^4 + \frac{c}{6}\xi^6\ \right], \qquad (4.14)$$

where the coefficients are given by

$$a = \frac{\tilde{g}_1}{8} - 2\tilde{J} = k_B T\left(\frac{e^{\tilde{\varepsilon}/k_B T} + 2}{2}\right) - 2\tilde{J} \quad , \tag{4.15}$$

$$b = \frac{\tilde{g}_3}{8} = -\frac{k_B T}{48}\left(e^{\tilde{\varepsilon}/k_B T} - 4\right)\left(e^{\tilde{\varepsilon}/k_B T} + 2\right)^2 \quad , \tag{4.16}$$

$$c = \frac{\tilde{g}_5}{8} = \frac{k_B T}{1280}\left(3e^{5\tilde{\varepsilon}/k_B T} - 40e^{3\tilde{\varepsilon}/k_B T} + 240e^{\tilde{\varepsilon}/k_B T} + 256\right). \tag{4.17}$$

When the temperature dependences are taken into account for $\tilde{\varepsilon}$ and $\tilde{J}$, which were introduced in §3.3, the transition point obtained from eq.s(4.14)-(4.17) is, as it should, consistent with that given by the direct calculation of the mean field equation (3.27). This is , together with some additional features of the system expressed by (4.15)-(4.17), given in Appendix A.

In the temperature range near the first order transition point, which we are just interested in, the coefficients $\tilde{J}$, b and c are considered to be temperature-independent and hereafter we regard them as constants. Retaining the temperature dependence only in the coefficient a, we may write the free energy density in eq.(4.14) as

$$\tilde{f}_\xi(\xi) = \frac{\kappa_1}{2}\left(\frac{\partial \xi}{\partial x}\right)^2 + f_\xi(\xi), \tag{4.18}$$

$$f_\xi(\xi) = \frac{1}{2}\alpha(T - T_0)\xi^2 + \frac{b}{4}\xi^4 + \frac{c}{6}\xi^6, \tag{4.19}$$

$$(\kappa_1 > 0 \ , \ \alpha > 0 \ , \ b < 0 \ , \ c > 0 \ ).$$

Here $\tilde{J}$ is replaced by the positive constant κ_1. The first term in eq.(4.18) stands for the energy due to spatial modulation of the order parameter. The reader should not confuse the free energy density (4.19) with the local potential (3.4). The former is a macroscopic quantity obtained by the coarse graining procedure while the latter is of microscopic. Note that f_ξ satisfies the symmetry property $f_\xi(-\xi)=f_\xi(\xi)$. This two-fold symmetry is essential to the low temperature structure with two variants of ordered phase. The characteristic feature of f_ξ is depicted in Fig.10.

We assume that in the temperature range of $T \gtrsim T_c$, there are chances that the order parameter ξ is locally (and temporally) 'locked' in the metastable state with $\xi = \bar{\xi}$. Since $\bar{\xi}$ gives the order parameter in the low temperature phase, the locally locked-in state with $\xi = \bar{\xi}$ may be called an embryonic fluctuation. The overall spatial variation of the order parameter $\xi(\mathbf{r})$ is obtained by the standard procedure to minimize the free energy functional under such boundary condition that embryonic fluctuations are excited randomly within the system.

4.2 Coupling to Strain

The structural transformation in solids is usually accompanied by a volume and/or shape change. In order to include this effect, strain energy contribution to the free energy should

be taken into account. The strain free energy density f_e associated with the longitudinal strain component e_{11} is given by

$$\tilde{f}_e(e_{11}) = \frac{\kappa_2}{2} (\frac{\partial e_{11}}{\partial x})^2 + f_e(e_{11}) , \qquad (4.20$$

$$f_e(e_{11}) = \frac{\chi}{2} e_{11}^2 , \qquad (\kappa_2 > 0 , \chi > 0), \qquad (4.21)$$

in which the energy increase due to the spatial variation of e_{11} is given by the first term in eq.(4.20).

In addition, we assume that there exists strong coupling between the order parameter ξ and the longitudinal strain component e_{11}. Taking into acount the translational invariance of each energy term, the lowest order coupling energy is given by

$$f_c(\xi, e_{11}) = \lambda e_{11}\xi^2 , \qquad (4.22)$$

where λ is a coupling coefficient.

Thus, combining all energy terms, the total energy functional is expressed by

$$F [\xi , e_{11}] = \int dr \{ \tilde{f}_\xi + \tilde{f}_e + f_c \} , \qquad (4.23)$$

$$= \int dr \{ \frac{\kappa_1}{2}(\frac{\partial \xi}{\partial x})^2 + \frac{\kappa_2}{2}(\frac{\partial e_{11}}{\partial x})^2 + U (\xi, e_{11}) \},$$

$$U (\xi , e_{11}) = f_\xi(\xi) + f_e(e_{11}) + f_c(\xi, e_{11}), \qquad (4.24)$$

where the potential function $U(\xi,e_{11})$ represents a homogeneous part of the free energy.

The feature of the transition of the system is most easily understood by drawing the potential surface within two-dimensional $(\xi\text{-}e_{11})$ space at various temperatures. We have chosen the coefficients in eq.(4.24) appropriately such that b=-140, c=4900, γ=1, and λ=-1 and have plotted the potential surface in Fig.11(a).

For later convenience, let us divide the temperature region into the following subregions depending on the characteristic of the potential function:

(I) $T_1 < T$; potential has single minimum at
$\boldsymbol{\xi}=(\xi,e_{11})=\mathbf{0}, T_1 = T_0 + \frac{g^2}{4\alpha c}$,

(II) $T_c < T < T_1$; triple minima at $\xi=0$,
and at $\boldsymbol{\xi}=\pm(\bar{\xi},\bar{e}_{11})=\pm\bar{\boldsymbol{\xi}}$,
the latter two are energetically
degenerate, ($U(\mathbf{0}) < U(\pm\bar{\boldsymbol{\xi}})$),

(III) $T_0 < T < T_c$; triple minima at the same positions as
those in (II), ($U(\mathbf{0}) > U(\pm\bar{\boldsymbol{\xi}})$),
$T_c = T_0 + \frac{3g^2}{16\alpha c}$,

(IV) $T < T_0$; double minima at $\boldsymbol{\xi}=\pm\bar{\boldsymbol{\xi}}$.

As is seen in Fig.11(a), at 'temperature' $\tau = \alpha(T-T_0) = 1.020$ $(= 1.322\ \tau_c)$, relatively well defined minimum is at $(\xi,e_{11})=(0,0)$. As τ is decreased there appears minimum at $(\xi,e_{11})=(\bar{\xi},\bar{e}_{11})$ in addition to the minimum at the origin. The former is metastable when $\tau \geqq \tau_c = 0.7717$, but becomes the

absolute minimum for $\tau < \tau_c$. The uniform ordered phase which is characterized by spatially uniform $\bar{\xi}$ and $\bar{e}_{11}$ with

$$\bar{\xi} = \frac{\beta + \sqrt{\beta^2 - 4\tau c}}{2c}, \qquad \left(\beta = |b| + \frac{2\lambda^2}{\chi} \right) \tag{4.25}$$

and $$\bar{e}_{11} = -\frac{\lambda}{\chi}\bar{\xi}^2 \quad , \tag{4.26}$$

is stabilized below the transition temperature.

We are particularly interested in the temperature region of $\tau_c < \tau < \tau_1$ (region (II)), because this region just corresponds to the precursor state. In this temperature regime, the stable state is of course given by $(\xi, e_{11})=(0,0)$. However, there may be finite possibility that the system <u>locally</u> surmount the potential barrier and is locked into the state $(\bar{\xi}, \bar{e}_{11})$ simply by thermal fluctuation. This locally ordered state should fluctuate back to the stable state (0,0) within finite lifetime. We may expect the lifetime would be substantially longer than the period of lattice vibration. That is, the local ordered state (embryonic fluctuation) is quasi-static in the scale of phonon frequency.

4.3 Solution for Embryonic Fluctuation

Let us consider that embryo is static and is sitting at a particular position $x = x_0$, and we investigate on the spatial variation of the order parameter $\xi(x)$ and strain $e_{11}(x)$ under the

particular boundary condition appropriate for the existence of the embryo:

$$\left.\begin{aligned} \xi &= \bar{\xi} \\ e_{11} &= \bar{e}_{11} \end{aligned}\right\} \text{ at } x = x_0 , \qquad \left.\begin{aligned} \xi &\to 0 \\ e_{11} &\to 0 \end{aligned}\right\} \text{ as } x \to \pm\infty . \tag{4.27}$$

We solve the following coupled Euler equations:

$$\left\{\begin{aligned} &-\kappa_1 \frac{\partial^2 \xi}{\partial x^2} + \frac{\partial U}{\partial \xi} = 0 \\ &-\kappa_2 \frac{\partial^2 e_{11}}{\partial x^2} + \frac{\partial U}{\partial e_{11}} = 0 \end{aligned}\right. \tag{4.28}$$

under the above boudary condition. From eq.(4.28), the first integral is readily obtained as

$$\left\{ \frac{\kappa_1}{2} \left(\frac{d\xi}{dx}\right)^2 + \frac{\kappa_2}{2} \left(\frac{de_{11}}{dx}\right)^2 \right\} - U(\xi, e_{11}) = U_0 , \tag{4.29}$$

where U_0 is an integral constant.

When $\kappa_2 = 0$, eq.(4.29) can be analytically solved for all temperature regions with appropriate boundary conditions. To get a feeling for the discussion below, it is worthwhile looking in a situation with $\kappa_2 = 0$. In region (II), the second boundary condition in eq.(4.27) requires $U_0 = 0$. Eq.(4.29) then becomes

$$\pm\sqrt{\frac{\tau}{\kappa_1}}\,dx = \frac{\frac{1}{2}\,d(\xi^2)}{\xi^2[1-\frac{\beta}{2\tau}\xi^2+\frac{c}{3\tau}\xi^4]^{1/2}} \quad . \tag{4.30}$$

This can be easily solved to give

$$\xi(x)= \frac{2\gamma e^{\sqrt{\tau/\kappa_1}\,(x-x_0)}}{[(2\sqrt{\frac{c}{3\tau}}-\frac{\beta}{2\tau})\gamma^4 e^{4\sqrt{\tau/\kappa_1}(x-x_0)}+\frac{\beta}{\tau}\gamma^2 e^{2\sqrt{\tau/\kappa_1}(x-x_0)}-(2\sqrt{\frac{c}{3\tau}}+\frac{\beta}{2\tau})]^{1/2}} \tag{4.31}$$

where the constant γ is determined by the first boundary condition in eq.(4.27) as

$$\gamma^2 = \frac{-(\frac{\beta}{2\tau}\bar{\xi}^2-2)+2(\frac{c}{3\tau}\bar{\xi}^4-\frac{\beta}{2\tau}\bar{\xi}^2+1)^{1/2}}{(2\sqrt{\frac{c}{3\tau}}-\frac{\beta}{2\tau})\bar{\xi}^2}. \tag{4.32}$$

The solution (4.31) just above τ_c (τ =0.772 ~ τ_c) is shown in Fig.12(a). In this case of κ_2= 0, $e_{11}(x)$ is given in terms of $\xi(x)$ as

$$e_{11}(x) = -\frac{\lambda}{\chi}\,\xi^2(x). \tag{4.33}$$

As τ approaches to τ_c, the spatial variations of $\xi(x)$ become kink-like, and eventually at $\tau = \tau_c$, $\xi(x)$ represents a kink (soliton) boundary solution (eq.(B.2)) which separates a low temperature embryo from the matrix phase.

It should be noted that the solution obtained in eq.(4.31) has somewhat unsatisfactory aspect in that $\partial\xi/\partial x \neq 0$ at $x=x_0$.

Since we are assuming that $\xi(x)=\xi(-x)$, the above situation implies that the spatial derivative at $x=x_0$, $d\xi/dx|_{x=x_0}$ is discontinuous, which is not physically plausible. This point will be discussed in §4.5.2

For the completeness of the discussion on the transformation, solutions to eq.(4.29) with $\kappa_2=0$ for other temperature regions, that are not concerned directly with the following discussion, are shown in the Appendix B, in which brief account of the transformation scheme using those solutions is also given. (See also Fig.12.)

In case when κ_2 is included, it is impossible to solve eq.(4.29) analytically. We have obtained numerically the solutions $\xi(x)$ and $e_{11}(x)$ following the iteration method developed by Ishibashi et. al.[46] with a little improvements for effective convergence. The eq.s (4.31) and (4.33) were taken as initial configurations and the eq.(4.29) was used to check whether the solutions were convergent or not. The calculated values of $\xi(x)$ and $e_{11}(x)$ are plotted in Fig.11(b).

The most interesting point of the numerical solutions is that, as τ is decreased, the functional forms of $\xi(x)$ and $e_{11}(x)$ bear different characteristics; $\xi(x)$ becomes more 'kink (soliton)'-like, having interface region between the embryo and the mother matrix. (Previously, Yamada et.al.[27] call the entity including the interface region a 'dressed embryo'.) On the other hand, $e_{11}(x)$ simply shows gradual decay around $x=x_0$.

It is instructive to draw the 'trajectory' within 2-D (ξ-e_{11}) space by eliminating the spatial coordinate x from the

solutions $\xi(x)$ and $e_{11}(x)$. This gives the lowest energy path from $(\bar{\xi},\bar{e}_{11})$ to (0,0) to be followed by the representative point of the system as x is varied. The trajectories at various temperatures are plotted on the equienergy contour maps (Fig.11(c)). Notice that the representative points in the figure are plotted at equal interval Δx of the coordinate x. Therefore, the density of the points along the trajectory directly reflects the length of persistence of the state in the real space. The high density region around $(\bar{\xi},\bar{e}_{11})$ corresponds to the embryonic fluctuation or the dressed embryo. In region (II), the total system should be expressed by random distribution of these embryonic fluctuations throughout the mother lattice.

4.4 Anomalous Incommensurability

As is discussed briefly in §2, X-ray scattering at the precursor state sometimes shows remarkable peculiarity as summarized in the following; Ni-Ti-Fe alloy, a well known shape memory alloy, undergoes phase transition with decreasing temperature from β_1 structure to a martensite phase through softening of TA phonon mode with $\mathbf{q}=1/3[110]$[19] (see Table I). Salamon[18] first reported that there appears an intermediate state where **q**-values of the superlattice reflections are incommensurate before they 'lock' into the exact commensurate value of 1/3 in the low temperature phase. By the high-resolution X-ray study Shapiro et.al.[19] found anomalous behavior associated

with the incommensurability of the satellite peaks: Not only they are incommensurate in position, but the incommensurability Δq changes from Brillouin zone to Brillouin zone. Moreover, the pair of peaks within a Brillouin zone does not satisfy center of symmetry around the Brillouin zone center, as usually does, but only maintain symmetry around the origin of the reciprocal lattice. These unusual symmetry properties of Δq definitely rule out the ordinary incommensurate structure with CDW's or LDW's, in which case satellites should satisfy the center of symmetry around each Brillouin zone center as well as the translational symmetry with respect to translation of Brillouin zones.

Salamon et.al.[22] pointed out very interesting feature on this anomalous incommensurability of the satellites in Ni-Ti-Fe; As is illustrated in Fig.13, the observed diffraction pattern can be systematically reproduced if we assume that only satellite peaks have shifted to the positions expected in the rhombohedral martensite phase, while the Bragg peaks still maintaining the original cubic positions. They referred to this peculiar reciprocal lattice as 'ghost lattice'. This 'ghost lattice' behavior was also found in the precursor state of Au-Cd.[20] Following Salamon et.al. when the relevant soft mode under consideration is the zone boundary mode (4.2), the 'ghost lattice' can be sketched as in Fig.14.

Yamada et.al.[27] constructed a possible microscopic model to explain the physical origin of the 'ghost lattice'. The basic idea of their model was that (i) the bcc matrix has a particular elastic property presented by a dip in TA phonon mode or the

presence of the 'soft mode' (§2.2.1(a)) and (ii) in the precursor state many 'embryos' or locally transformed microregion of low temperature structures are distributed in the matrix. They set up model system of 1-D and 2-D lattices of atoms whose phonon dispersion has soft phonon modes. The displacement field was then calculated when the lattice is strained by a specific type of Kanzaki force[47] which stands for the existence of embryos and found that the lattice relaxation around the embryo gives modulation corresponding to the soft mode. They showed that the diffraction pattern of this spontaneously strained lattice indeed reproduces the characteristics of the 'ghost lattice', i.e., that the modulated lattice relaxation (MLR) around each embryo are essential to produce anomalous incommensurability of the satellite shifts in the diffraction pattern.

Although their treatment elucidated possible origin of the 'ghost' behavior, the discussion based on such specific lattice dynamical model left the point of generality and overall applicability of the idea unclear. In this subsection we will discuss the same problem utilizing the phenomenological argument developed in the preceding subsections.

It is straightforward to obtain the diffraction pattern using the calculated values of $\xi(x)$ and $e_{11}(x)$ in the preceding subsection. Using eq.(4.1), displacement of the n-th atom associated with $\xi(x)$ is given by

$$\mathbf{u}_t(n) = \mathbf{e}(\mathbf{q}_0)\, \xi(n\mathbf{a})\, e^{i\, \mathbf{q}_0 \cdot n\mathbf{a}} + \text{c.c.} \quad . \tag{4.34}$$

In addition, we have the longitudinal component due to the strain field $e_{11}(x)$,

$$\mathbf{u}_l(n) = \mathbf{e}_s\, e_{11}(n\mathbf{a}) \ , \quad \mathbf{e}_s // \mathbf{a} \quad . \tag{4.35}$$

The diffraction spectrum $S(\mathbf{K})$ is obtained by

$$S(\mathbf{K}) = F(\mathbf{K})\, F^*(\mathbf{K}) \quad , \tag{4.36}$$

$$F(\mathbf{K}) = \sum_n e^{i\,\mathbf{K}\cdot(n\mathbf{a} + \mathbf{u}_n)} \quad , \tag{4.37}$$

$$\mathbf{u}_n = \mathbf{u}_t(n) + \mathbf{u}_l(n) \quad . \tag{4.38}$$

In the calculation of the spectrum we neglect, for simplicity, the atomic scattering factor as well as the Debye-Waller factor. The calculated profiles of S(hk0) (k=1) are given in Fig.15.

There are several important characteristics in the calculated spectra:

(1) Throughout temperature range $1 \lesssim \tau/\tau_c < 1.322$, the satellite peaks shift toward the origin of the reciprocal lattice, increasing the amount of shift as $|\mathbf{K}|$ is increased, while the fundamental Bragg peaks stay at the original regular positions. (See Fig.16.)

(2) As the temperature is lowered below $\tau < 1$ ($\tau/\tau_c \lesssim 1.3$), the profile of the higher order satellite peaks starts to show complicated structure. Particulary it tends to split into two

peaks where the second peak seems to restore the commensurate positions.

(3) The Bragg peaks show appreciable tailing which is convensionally called Huang scattering[47] due to defects of various kinds.

The characteristics (1) of course gives that of the 'ghost lattice' or anomalous incommensurability. It is noticeable, however, that the satellite peak positions are approximately half way between the commensurate positions of the high temperature and the low temperature lattices which are on the two straight lines given in Fig.16.

The physical origin of the 'ghost lattice' is now clear; The strain field $e_{11}(x)$ around $x=x_0$ is essentially same as those of a 'defect' such as impurity, vacancy, etc. The resultant diffraction effect is Huang scattering around the Bragg peak which gives tailing but not shift of the peak positions. The embryonic fluctuation $\xi(x)$, on the other hand, gives rise to superlattice reflections. If there were no strain, the peak positions should be at the commensurate positions associated with the Bragg peaks. However, in the spatial region where $\xi(x) \neq 0$, the strain field has also appreciable values, which means that the embryonic fluctuations are preferentially embedded on the lattice with larger lattice constant; $a_0(1+1/2\ \bar{e}_{11})$ on average. Thus the satellite peak positions are at $1/2\ h(1-1/2\ \bar{e}_{11})a_0^*$ rather that at $1/2\ ha_0^*$.

4.5 Summary and Discussion

4.5.1 Summary of Results and Comparison with Experimental Results

We have 'materialized', so to speak, the 'ghost' by identifying that the origin of the anomalous incommensurability is due to embryonic fluctuation which is coupled strongly to the strain. The discussion is based on the general expression of free energy functional characterizing first order phase transition. Therefore the results are not restricted by microscopic lattice dynamical model as previously assumed in the case of β-based alloys.[27] In principle, any crystal system undergoing first order phase transition and satisfying the above condition (existence of strong coupling of order parameter to strain) would show 'ghost lattice' behavior. More precise experimental investigations on various substances are certainly necessary.

As is described in the previous subsection, one of the important characteristics of the calculated pattern is that the profile of higher order satellites starts to split into two peaks as the tempertarue is lowered below $\tau < 1$ ($\tau/\tau_c \lesssim 1.3$). The secondary peaks are approximately on the commensurate positions. In the previous investigations on bcc metals Ni-Ti-Fe[19] and Au-Cd,[20] the satellite did show anomalous broadening but not splitting. Recently, however, Kiat et.al.*7 observed definite

---

*7 Private communication.

splitting of satellites while fundamental Bragg peaks remain single peaks above the ferroelastic transition of $Pb_2(PO_4)_3$ crystal. This might be understood in terms of the characteristic feature described above.

Next we discuss the relation between our results for the 1-D system and experimentally observed shift pattern of satellite reflections in 2-D reciprocal space. Notice the results presented in §4.4 was calculated for the case in which $\lambda<0$. If we take $\lambda>0$, from the analogy to $\kappa_2= 0$ case (eq.(4.26)), then the longitudinal strain will be a contraction toward the embryo center, which results in a similar diffraction profile to those shown in Fig.15 except that the direction of the shift is reversed. That is, all of the superlattice reflections shift away from the origin of the reciprocal lattice. If we extend the model to two-dimensional system in which λ is allowed to be orientation-dependent in such a way that λ is negative in one direction and is positive in the other which is perpendicular to the former. This spatial dependence of the sign of λ may be expected to exist due to the intrinsic unisotropy of the parent structure. We can thus reproduce overall 'swirl' shift pattern of superlattice reflections observed in Ni-Ti-Fe[19] and Au-Cd.[20]

4.5.2 Limit of Our Approach

Let us now discuss some problems still remaining in our treatment; The present treatment is based on the assumption that

the system will be locally locked-in at $\bar{\xi}=(\bar{\xi},\bar{e}_{11})$ by thermal activation. Let us consider the 'creation energy' $E(\xi_0)$ of an embryonic fluctuation with an arbitrary amplitude ξ_0 at $x=x_0$. This was already discussed by Falk[48] in a simpler case (no coupling between the order parameter to some other physical quantities). Following similar procedure given by Falk, it is easy to show that the creation energy is monotonically increasing with increasing ξ_0. Therefore, against our assumption, there seems to be no particular reason for the system to lock-in to the value of $\bar{\xi}$ even locally as far as the energy given in eq.(4.23) is concerned.

This point seems to be closely related to the inadequacy of the solution $\xi(x)$ in the region (II). As has been pointed out in §4.3, $d\xi/dx$ is discontinuous at $=x_0$ which is certainly unphysical. The most probable modification of the theoretical scheme to get rid of this inadequacy would be obtained by including higher order derivatives such as $(\partial^2\xi/\partial x^2)^2$ in the free energy density. That is, it will be necessary for describing correctly the immediate neighborhood of the embryo center to keep shorter wave length fluctuations upon evaluating the free enegy. We expect that when this singularity is removed by including higher order derivative terms, $E(\xi_0)$ would have a local minimum at $\xi_0\simeq\bar{\xi}$.

The careful reinvestigation of the validity of the boundary conditions to be imposed is certainly necessary. In connection with this point, we refer to Falk's treatment. In region (II), he has given a solution which is quite different from our dressed

embryo picture. His solution is characterized by: $\xi \to \bar{\xi}$, $d\xi/dx \to 0$, as $x \to \pm\infty$. The major reason of the difference resides in the choice of U_0. In our treatment, we have chosen $U_0 = 0 + \varepsilon$ (with ε an infinitesimal positive value), while it was to taken to be a finite positive value in Falk's treatment.

4.5.3 Future Problems

We have considered in this section that the embryonic fluctuation is a static entity. However, the lifetime of the embryonic fluctuation should be finite as has been stated in §2 and, hence, it is certainly necessary for the correct description of the system above the transition temperature to deal with the dynamics of the system. The dynamical problem associated with this particular system having long-lived embryonic fluctuation may be divided into two parts; the dispersive and the dissipative problems.

The former put the lattice dynamical property in question. As was mentioned in §2.2.1 there is already the anomaly in the lattice dynamical property of the parent lattice; a dip in phonon dipersion curve. The existence of the embryonic fluctuations may also affect the lattice dynamical property of the system. Besides the above anomaly in phonon dispersion curve, extra excitation forming subsidiary branches in addition to ordinary phonon branches have been observed in diffuse ω-phase in Zr-Nb alloy.[16,49] Although this phenomena may be closely related to

the lattice instability against TA_2 phonon mode with $q=1/3[211]$ and $e//[\bar{1}11]$ (see Tabel I) and the existence of the embryonic fluctuations, a satisfactory explanation has not yet been given. We speculate, however, that this new excitation may be ascribed to the lattice dynamical property within the embryonic fluctuation, which depends on the curvare of metastable minimum of the local potential V_{loc}. To check this it is effective to start with the hamiltonian in the form of eq.s(3.1)-(3.3), with suitable form for V_{loc} to have triple minimum as eq.(3.4).

The latter, on the other hand, deals with the relaxation of embryonic fluctuations, in which nucleation, annihilation and coagulation processes of embryonic fluctuations are involved. A time-dependent-Ginzburg-Landau approach[50] with the GL free energy (4.14) will be useful to this problem, by which a quantitaive discussion can be made on, for example, the central peak problem (§2.2.1).[15,51]

§ 5. CONCLUSION

We have discussed on the precursor phenomena and ensuing martensite phase transformation (or similar general first order phase transformations in solids) based throughout on the idea that the key mechansism of these phenomena is attributable to the motion of locally excited long-lived tristable fluctuations, which we called 'embryonic fluctuations'. Precursor phenomena which appear as various anomalies in the physical properties above the transition temperature are reviewed in this context. Based on this idea we have developed a semimicroscopic treatment. Various features of the martensite transformation are successfully explained including precursors in terms of embryonic fluctuations. In particular, application to Ni-Al 7R structure has proven that the present approach is quite effective to elucidate the ground state structure in the martensite phase.

A thermodynamical viewpoint has been also establised by deducing the expression of free energy functional. Embryonic fluctuations are obtained as the thermodynamcially metastable state just above the first order transition point, if we assume particular boundary conditions to determine the space variation of the order parameter.

Finally let us emphasize an underlying significance of the physical meaning of the precursor state associated with the first order phase transitions. As has been mentioned in introduction order parameters describing the second order phase transitions can be specified either by some soft phonon modes or by classical

bistable pseudospin modes, and the associated critical phenomena are characterized by the critical divergence of the correlated fluctuations of these modes.

The precursor phenomena are quite different from those critical phenomena, because the former are associated with the metastable state of tristable fluctuations, which inevitably introduce strong nonlinearity in the system. Our macroscopic treatment presented in §4 may be viewed as one of the challenges to these difficulties, though incomplete in that we have treated the embryonic fluctuations as completely static. The concept of the embryonic fluctuations may provide a wholly new aspect of the understanding of first order phase transition, whose formulation of the framework has just begun.

APPENDIX A

Transion Points Obtained from The Free Energy (4.14)

Before calculating the transition points let us evaluate the sign of each coefficient. Since $e^{\tilde{\varepsilon}/k_BT} > 0$ irrespective of the temperature-dependence of $\tilde{\varepsilon}$, the coefficient c is easily proved to be positive definite from eq.(4.17). On the contrary, as is seen from eq.(4.16), the coefficient b can change its sign as follows;

$$\text{if} \quad e^{\tilde{\varepsilon}/k_BT} \gtrless 4 , \quad \text{then} \quad b \lessgtr 0 . \tag{A.1}$$

The condition $a = 0$ yields a transition point T_c when the transition is of second order. This can be read from eq.(4.15) as

$$\frac{4\tilde{J}(T_c)}{k_BT_c} = e^{\tilde{\varepsilon}(T_c)/k_BT_c} + 2 . \tag{A.2}$$

Note that eq.(A.2) agrees, as it should, with the condition of the second order phase transition point directly obtainable from the mean field eq.(3.27) through the equation

$$\frac{\partial}{\partial\langle\sigma\rangle}[\text{ r.h.s. of (3.27) }]\,|_{\langle\sigma\rangle=0} = 1 \tag{A.3}$$

with z=2.

On the other hand, the transition point when the transition is of <u>first order</u> is obtained from the situation in which both heights of absolute minimum and metastable minimum of the free energy density are equal. This situation can be expressed in terms of those coefficients as

$$16ac = 3b^2 \ . \qquad (A.4)$$

The system described by the free enegy (4.14) thus has a possibility that, depending on the temperature-dependences of $\tilde{\varepsilon}$ and $\tilde{J}$, first or second order phase transitions may take place. To inquire this possibility more quantitaively, the same temperature-dependences for ε and κ appear in the coefficients are assumed here as were used in §3.4. Using the same notation as that was used in §3.4,

$$e^{\tilde{\varepsilon}(T)/k_BT} = e^{\tau - \gamma/\tau^2} \ , \quad (\gamma > 0) \qquad (A.5)$$

$$\tilde{J}\beta = \gamma / \tau^2 \ . \qquad (A.6)$$

One can soon notice that from eq.(A.5) $e^{\tau - \gamma/\tau^2}$ diverges as $\tau \to \infty$ and tends to zero as $\tau \to 0$. From this fact, together with (A.1), one can show the following;

$$\begin{aligned} &{}^{\exists}\tau_0 = \tau_0(\gamma) > 0, \text{ uniquely} \\ &\text{st on } \tau \gtrless \tau_0 \ , \quad b \gtrless 0 \ . \end{aligned} \qquad (A.7)$$

In addition, the unique existence of $\tau_1(>0)$ such that

$$\text{on} \quad \tau \gtrless \tau_1 \quad , \quad b^2-4ac \lessgtr 0 \tag{A.8}$$

is also shown. Noting that the necessary and sufficient condition for the homogeneous part of the free energy density in eq.(4.14) to have triple minima is $b < 0$ and $b^2-4ac > 0$, the first order transition can take place in the case where $\tau_0(\Upsilon_c)<\tau_1(\Upsilon_c)$. Conversely speaking, if the transition occurrs in such a case that $\tau_0(\Upsilon)>\tau_1(\Upsilon)$, then the transition should be of second order. Therefore, the condition

$$\tau_0(\Upsilon_m) = \tau_1(\Upsilon_m) \tag{A.9}$$

yields implicit determination of the parameter Υ corresponds to a crossover region between first and second order phase transitions. The value of Υ_m is numerically estimated as $\Upsilon_m \simeq 12.5$. The transition points are then calculated either from eq.(A.2) or eq.(A.4) for two values of Υ, between which Υ_m is to be interposed, and the results are tabulated in Table II, together with the results obtained by the direct calculation from the mean field eq.(3.27).

APPENDIX B

Exact Solutions of Eq.(4.27) for Temperature regions III, IV When $\kappa_2=0$

We give here exact solutions to eq.(4.27) when $\kappa_2 = 0$ for other temperature regions.

At T_c, $16\,\tau c = 3\,g^2$ holds. $U(\xi, e_{11})$ then becomes

$$U(\xi, e_{11}) = \left(\sqrt{\frac{\tau}{2}}\,\xi - \sqrt{\frac{c}{6}}\,\xi^3 \right)^2 , \qquad (B.1)$$

which is now inserted to eq.(4.27). Using the boundary condition $U_0 = 0$, eq.(4.27) is readily integrated to give

$$\xi(x) = \pm\left[\frac{e^{\pm 2\sqrt{\tau/\kappa_1}\,(x-x_0)}}{1 + \frac{1}{\bar{\xi}^2}\, e^{\pm 2\sqrt{\tau/\kappa_1}\,(x-x_0)}} \right]^{1/2} . \qquad (B.2)$$

If we take plus sign in front of the brackets, then $\xi(x)$ represents a phase boundary which separates from the matrix an embryo with the amplitude $\bar{\xi}$ at the embryo center, and if we take minus sign, $\xi(x)$ is a boundary separating an embryo of the other variant whose amplitude at the embryo center is equal to $-\bar{\xi}$. In the former if we take plus(minus) sign in the brackets, then the boundary is a (an anti-) kink (shown in Fig.12(b) is the latter) while in the latter the results would be interchanged.

Below T_c (region (III),(IV)) the situation will change; we have to replace physically plausible boundary conditions as

$$\xi \to -\bar{\xi} \quad \text{as} \quad x \to -\infty\,, \quad \xi \to \bar{\xi} \quad \text{as} \quad x \to \infty$$

or (B.3)

$$\xi \to \bar{\xi} \quad \text{as} \quad x \to -\infty\,, \quad \xi \to -\bar{\xi} \quad \text{as} \quad x \to \infty.$$

The corresponding U_0 to (B.3) is $U_0 = -\bar{U} = -U(\bar{\xi}, e_{11}(\bar{\xi}))$. Since

$$U(\xi_{11}, e_{11}) - \bar{U} = \frac{c}{6}(\Xi - \bar{\Xi})^2(\Xi + 2\bar{\Xi} - \frac{3\beta}{2c}) \,, \tag{B.4}$$

where $\Xi = \xi^2$, $\bar{\Xi} = \bar{\xi}^2$, eq.(4.27) becomes

$$\frac{1}{2} \frac{d\Xi}{\sqrt{\frac{c}{6}}\,[(\Xi+2\bar{\Xi}-\frac{3\beta}{2c})\,\Xi\,(\Xi-\bar{\Xi})^2]^{1/2}} = \pm\sqrt{\frac{2}{\kappa_1}}\,dx \tag{B.5}$$

Using the elliptic integral of the first kind, eq.(B.5) is integrated to give

$$F(\Phi, k=1) = \pm\sqrt{\bar{\Xi}(\bar{\Xi}-\frac{\beta}{2c})\frac{c}{\kappa_1}}\,(x-x_0),$$

(B.6)

$$\Phi = \sin^{-1}\sqrt{\frac{3\bar{\Xi} - \frac{3\beta}{2c}}{\bar{\Xi}}\,\frac{\Xi}{\Xi+2\bar{\Xi}-\frac{3\beta}{2c}}}\,.$$

Taking the inverse function,

$$\Phi = \text{am}\,(\,\pm\sqrt{\bar{\Xi}(\bar{\Xi} - \frac{\beta}{2c})\frac{c}{\kappa_1}}\,(x_0 x)\,,\ k = 1\,)$$

$$= \tan^{-1} \sinh \left(\pm\bar{\Xi} \sqrt{(1 - \frac{\beta}{2\bar{\Xi}c})\frac{c}{\kappa_1}} (x-x_0) \right) \qquad (B.7)$$

Upon solving for $\bar{\Xi}$ and then taking a root, $\xi(x)$ can be obtained as

$$\xi(x) = \pm \frac{\bar{\xi}\sqrt{2-\frac{3\beta}{2\bar{\Xi}c}} \sinh\bar{\Xi}\sqrt{(1-\frac{\beta}{2\bar{\Xi}c})\frac{c}{\kappa_1}} (x-x_0)}{\left[3-\frac{3\beta}{2\bar{\Xi}c} + (2-\frac{3\beta}{2\bar{\Xi}c}) \sinh^2\bar{\Xi}\sqrt{(1-\frac{\beta}{2\bar{\Xi}c})\frac{c}{\kappa_1}} (x-x_0)\right]^{1/2}} \qquad (B.8)$$

where $\xi(x)$ is a (an anti-) kink if the plus (minus) sign is chosen. In eq.(B.8) only the solution representing an antikink is shown in Fig.12(c).

Note that from eq.s(4.31), (B.2) and (B.8), one can easily imagine the phase transfomation process (see Fig.B.1); Above τ_c there appear embryonic fluctuations by thermal activation, but the density of embryos is so dilute that the form of a single embryo is well expressed by eq.(4.31) (Fig.B.1(a)). The boundary between an embryo and the matrix becomes clearer as $\tau \to \tau_c$. Since due to the symmetric property of the system the exisitence of an embryo of the other variant is also allowable. At τ_c the boundary of the former becomes a kink-antikink pair (eq.(B.2)) of one kind of variants whereas the boundary of the latter will be that of the other kind (Fig.B.1.(b)). The kinks with the opposite signs will annihilate to form a large domain of the one kind while the kinks with the same signs will collapse to form an antiphase boundary which separates two variants (eq.(B.8), Fig.B.1(c)).

Then an effective interaction between those antiphase boundaries is expected to come into play, as that between discommesurations in the incommesurate structure,[45] by which an alternative arrangement of different variants realizes below T_c. This arrangement of variants is one of characteristic features usually observed in martensite structure (Fig.B.1(d)).

In this way, the tentative explanation of the transfomation process according to the MLR picture presented in §2.2.1 can be confirmed by using these solutions.

ACKNOWLEDGEMENTS

The author would like to express his gratitudes to Prof. Y. Yamada of the Institute for Solid State Physics, University of Tokyo for continuous guidance in the present investigation and for careful reading the manuscript. He wishes to thank Prof. T. Ohta and Miss H. Nozaki of Ochanomizu Women's University for performing preliminary calculations for him. Thanks are also due to Dr.S.M.Shapiro and Dr.G.Shirane of Brookhaven National Lboratory and Dr.L.E.Tanner of Lawrence Livermore National Laboratory for providing the author with their experimental data prior to publication. Hearty thanks are due to Dr.N.Hamaya, Dr. Y.Noda, Profs.Y.Fujii and S.Nasu of Osaka University and Dr.T. Kawakatsu of Kyusyu University for many enjoyable discussions and encouragements throughout the course of this study. Prof. A. Yoshimori of Osaka University gave the author very useful comments. Special thanks are due to Prof.F.E.Fujita of Osaka University whose critical and throughout review resulted in numerous improvements. All numerical calculations presented were made at Data Processing Center, Kyoto University.

REFERENCES

1) H.Unoki and T.Sakudo: J. Phys. Soc. Jpn. **23**(1967) 546.
G.Shirane and Y.Yamada: Phys. Rev. **177**(1969) 858.
J.Harada, T.Pedersen and Z.Barnea: Acta Crystallogr. A**26**(1970) 336.
See also Ref.4 and references cited therein.

2) W.Cochran: Adv. Phys. **9**(1960) 387.

3) P.W.Anderson: Fizika Dielectrikov, ed. G.I.Skanavi (Acad. Nauk. SSR., Moscow, 1960).

4) J.F.Scott: Rev. Mod. Phys. **46**(1974) 83.
G.Shirane: ibid. **46**(1974) 437.

5) S.Hoshino and H.Motegi: Jpn. J. Appl. Phys. **6**(1967) 708.

6) See, for exmaple, H.E.Stanley: Introduction to Phase Transitions and Critical Phenomena (Clarendon Press, Oxford, 1971).

7) Z.Nishiyama: Martensitic Transformations (Academic Press, New York, 1978).
For a review, see, A.L.Roitburd: Solid State Physics **33**(1978) 317.

8) N.G.Pace and G.A.Saunders: Solid State Commun. **9**(1971) 331.
T.R.Finlayson: Met. Trans. **19**A(1988) 185.

9) T.R.Finlayson and H.G.Smith: ibid. 193.
T.R.Finlayson, A.J.Morton and P.D. Norman: ibid. 199.
M.Wuttig, C.Y.Lei and T.Suzuki: ibid. 789.
A.Nagasawa, T.Makita, N.Nakanishi, M.Iizumi and Y.Morii: ibid. 793.

10) L.E.Tanner, A.R.Pelton and R.Gronsky: J.Phys.(Paris) Colloq.**43**(1982) C4-169.
L.E.Tanner: Proc. Symp. Competing Interactions and Microstructures, Springer Series Sol.-St.Sci. (Springer-Verlag, 1988) in press.
R.Oshima, M.Sugiyama and F.E.Fujita: Met. Trans. **19A**(1988) 803.

11) S.Mendelson: Met. Trans. **19A**(1988) 811, and references therein.

12) K.Otsuka, C.M.Wayman and H.Kubo: Met. Trans. **9A**(1978) 1075.
I.M.Robertson and C.M.Wayman: Met. Trans. **15A**(1984)69.

13) M.Mori, Y.Yamada and G.Shirane: Solid State Commu. **17**(1975) 127.

14) S.M.Shapiro, J.Z.Larese, Y.Noda, S.C.Moss and L.E.Tanner: Phys. Rev. Lett. **57**(1986) 3199.

15) G.Shirane and J.D.Axe: Phys. Rev. Lett. **27**(1971) 1803.

16) S.C.Moss, D.T.Keating and J.D.Axe: Phase Transitions-1973, ed. L.E.Cross (Pergamon, New York, 1973) p.179.
J.D.Axe, D.T.Keating and S.C.Moss: Phys. Rev. Lett. **35**(1975) 530.

17) K.Otsuka, T.Sawamura and K.Shimizu: Phys. St. Sol. **5**(1971) 457.
G.D.Sandrock, A.J.Perkins and R.F.Hehemann: Met. Tran. **2**(1971) 2769.
G.M.Michal, P.Moine and R.Sinclair: Acta Met. **30**(1982) 125.

18) M.B.Salamon, M.Meichle, C.M.Wayman, C.M.Huang and S.M.Shapiro: Int. Conf. Modulated Structures, AIP Conf.

No.53, ed. J.M.Cowley, J.B.Cohen, M.B.Salamon and B.J.Buensch (AIP, New York, 1979) p.223.

19) S.M.Shapiro, Y.Noda, Y.Fujii, and Y.Yamada: Phys. Rev. B**30**(1984) 4314.

20) Y.Noda, M.Takimoto, T.Nakagawa, and Y.Yamada: Met. Trans. **19**A(1988) 265.

21) M.Matsumoto and T.Honma: Proc. Int. Conf. Martensite (Kobe, Japan, 1976) p.199.

22) M.B.Salamon, M.E.Meichle and C.M.Wayman: Phys. Rev. B**31**(1985) 7306.

23) C.Zener: Phys. Rev. **15**(1947) 846.

24) J.A.Krumhansl: Nonlinearity in Condensed Matter, ed. A.R.Bishop, D.K.Compbell, P.Kumar and S.E.Trullinger, Springer Series Sol.-St.Sci.**60** (Springer-Verlag, 1986) p.255, and references therein.

25) P.C.Clapp: Phys, Stat. Sol. (b)**57**(1973) 561.
G.Guenin and P.F.Gobin: Met. Trans. **13**A(1982) 1127.
G.Guenin and P.C.Clapp: Proc. Int. Conf. Martensite, Nara, 1986 (Jpn. Inst. Met., Tokyo, 1986) p.171.

26) J.P.Hirth and J.Lothe: Theory of Dislocation (John Wiley, New York, 1982) 2nd ed., p.315.

27) Yamada, Y.Noda, M.Takimoto, and K.Furukawa: J. Phys. Soc. Jpn. **54**(1985) 2940.
Y.Yamada, Y.Noda and M.Takimoto: Solid State Commun. **55**(1985) 1003.
Y.Yamada: Met. Trans. **19**A(1988) 777.

28) T.Suzuki and M.Wuttig: Acta Met. **23**(1975) 1069.

29) P.C.Clapp, J.Rifkin, J.Kenyon, and L.E.Tanner: Met. Trans. **19A**(1988) 783.

A.Silberstein and P.C.Clapp: Phys. Rev. B**38**(1988) 9555.

30) W.J.Buehler, J.V.Gilfrich and R.C.Wiley: J. Appl. Phys. **34**(1963) 1475.

C.M.Wayman: Physical Metallurgy, ed. J.W.Cahn and P.Haasen (Elsevier, Amsterdam, 1983) 3rd ed., Chap.15.

31) S.Mendelson: Mater. Sci. Engr. **81**(1986) 107.

32) For a review, see, A.D.Bruce: Adv. Phys. **29**(1080) 111.

33) Y.Onodera: Prog. Theor. Phys. **44**(1970) 1477.

34) P.C.Kwok and P.B.Miller: Phys. Rev. **151**(1966) 387.

35) T.H.K.Barron and M.L.Klein: Dynamical Properties of Solids, vol.1, ed. G.K.Horton and A.A.Maradudin (North-Holland Publishing Co., Amsterdom, 1974) Chap.7.

36) A.Nagasawa: J. Phys. Soc. Jpn. **40**(1976) 1021.

37) J.L.Smialek and R.F.Hehemann: Met. Trans. **4**(1973) 1571.

38) V.V.Martynov, K.Enami, L.G.Khandros, S.Nenno, and A.V.Tkachenko: Phys. Met. Metall. **55**(1983) 136.

39) S.M.Shapiro, B.X.Yang, G.Shirane, Y.Noda, and L.E.Tanner: to be published.

40) D.Schryvers, L.E.Tanner and S.M.Shapiro: Proc. MRS Symp. Shape Memory Materials, Int. Mtg. Adv. Mtls. 88-89 (MRS, Pittsburgh, 1988) in press.

41) S.Hendricks and E.Teller: J. Chem. Phys. **10**(1942) 147.

42) R.J.Gooding and J.A.Krumhansl: Phys. Rev. B**38**(1988) 1695.

43) R.J.Gooding and J.A.Krumhansl: to be published.

44) R.Berliner and S.A.Werner: Phys. Rev. B**34**(1986) 3586.

45) P.Bak and J.von Boehm: Phys. Rev. B**21**(1980) 5297.

46) Y.Ishibashi and V.Dvorak: J. Phys. Soc. Jpn. **44**(1978) 32.

47) P.H.Dederichs: J. Phys. F**3**(1973) 471.

48) F.Falk: Z. Phys. B**51**(1983) 177.

49) Y.Noda, Y.Yamada and S.M.Shapiro: to be published.

50) M.Buttiker and R.Landauer: Phys. Rev. Lett. **43**(1979) 1453.
M.Buttiker and R.Landauer: Phys. Rev. A**23**(1981) 1397.

51) J.A.Krumhansl and J.R.Schrieffer: Phys. Rev. B**11**(1975) 3535.

Table I

Soft phonon modes and resultant low temperature hexagonal based structures. Note that the so-called ω-phase structure can be included in a category of martensitic transformation in view of the displacive nature upon the transformation.

soft mode q_0	soft mode e	low temp. structure	exmaple
1/2<110>	<1$\bar{1}$0>	2H martensite	Cu-Al-Ni[a]
1/3<110>	<1$\bar{1}$0>	9R martensite	Au-Cu-Zn[b]
~1/7<110>	<1$\bar{1}$0>	'7R'martensite	Ni-Al[c]
δ<110> δ~0	<1$\bar{1}$0>	B19	Nb_3Sn[d]
1/3<211>	<1$\bar{1}$0>	ω-phase	Zr-Nb[e]

[a]Ref.12.

[b]Ref.13.

[c]Ref.14.

[d]Ref.15.

[e]Ref.16.

Table II

Transition points obtained from the criteria (A.2) and (A.4). Those calculated directly by eq.(3.27) are also shown for comparison.

γ	τ_c from	τ_c from eq.(3.27)
0.4	.7320 eq.(A.2)	.7320
20	3.380 eq.(A.4)	3.389

FIGURE CAPTIONS

Figure 1. Schematic illustration of the micro(semimicro)scopic model. The atoms interact through a harmonic nearest neighbor coupling with a coupling constant K and also reside in a single particle potential V_{loc} having triple minimum. The displacement u of an atom is defined with repect to the high temperature phase equilibrium position represented by the central minimum of V_{loc}. An 1-D lattice with period a_0 is shown.

Figure 2. Schematic illustration of the construction process of martensite structure from a bcc(β) or a CsCl(β') lattice. In the following simar figures, the large open circles denote the A type atoms on the plane of z=0 and small full circles the B type atoms on the plane of z=1/2. (a) Atomic arrangement in the condensed state of a TA phonon with $\mathbf{q}=\mathbf{q}_0$ ($\mathbf{q}_0$//[110],$\mathbf{e}$//{1$\bar{1}$0]), which then forms locally the fcc structure caused by the further displacements of atoms indicated by the arrows. (b) The chain of fcc 'clusters' (enclosed by the thick lines). One of the 'cluster' is indicated by hatched region. Note that strains at the cluster boundaries reslut from the process (a) can be removed by the relative slips of the cluster with appropriate amounts in the directions shown by the arrows. (c) The resultant martensite structure. The same cluster chain as indicated in (b) is shown by the dashed lines.

Figure 3. Assignment of a spin variable to 3 types of cluster states; $\sigma=0$ stands for the undeformed cluster state and $\sigma=\pm1$ for the tilted cluster states.

Figure 4. (a) Schematic illustration of the model composed of clusters (hatched region) connected by harmonic springs with sping constant κ. Only two consecutive clusters with states, for example, $\sigma=0$ and $\sigma=1$ are shown. (b) The corresponding local potential-spring model. (See also the caption of Fig.1.)

Figure 5. The calculated variation of the order parameter $<\sigma>$ (solid line) and of the embryo density $<\sigma^2>$ (dashed line) with temperature. The abscissa is normalized by τ_c. Notice $<\sigma^2>$ remains finite even above τ_c and gradually decreases as the temperature is increased. In the inset, the experimental result by the X-ray diffraction in AuCd (Ref.) is shown for comparison.

Figure 6. Schematic illustration of the construction process of 9R martensite. (a) Atomic arrangement in the condensed state of a TA phonon with $q_0=1/3[110]$. Arrows indicate the further displacements of atoms introduced to form locally the fcc structure. (b) The chain of fcc 'clusters' embedded in the resultant structure. Arrows indicate the relative slips of the cluster to take place at the cluster boundaries in the $[1\bar{1}0]$ direction. The amount of the relative displacement of the cluster due to the slip is 1/6. (c) The resultant 9R structure. The

rectangle enclosed by the solid line is the unit cell of the 9R structure.

Figure 7. Schematic illustration for the formation of the cluster (embryo) when $\mathbf{q}_0$=1/7[110]. (a) Dashed lines represent the small amplitude phonon condensed state with $\mathbf{q}_0$=1/7[110]. Further displacements of atoms to form local fcc clusters are indicated by the arrows, which result in (b) a postulated cluster composed of six (110) layers (shown by the shaded area).

Figure 8. Schematic illustration of the costruction process of the martensite structure of Ni-Al. (a) See captions of Fig.7. (b) Clusteres are shown by the thick lines. Slips are troduced at the cluster boundaries in the directions indicated by the arrows. In this case the amount of the relative displacement due to the slip is 1/4. (c) The resultant martensite structure, which is essentially identical to the sao-called (5-$\bar{2}$) structure as is demonstrated in (c´). The rhomboid enclosed by the thick line in (c´) is the monoclinic unit cell. Note that resultant structure is viewed as alternative stacking of a distorted fcc and a distorted bcc slab. (See also the text.)

Figure 9. Comparison between the calculated (below) and the experimental intensity profile (Fig.2 of Ref.).

Figure 10. Schematic illustration of potential function f_ξ describing the first order phase transition . The abscissa

represents the order parameter ξ. Note that the states corresponding to $\xi=\pm\bar{\xi}$ (at which the potential have local minima) are energetically degenerate, which is essential to the low temperature ($T<T_c$) structure with two variants of ordered phase.

Figure 11(a). Potential surfaces within (ξ,e_{11}) space at various temperatures; from above, τ = 1.020 (= 1.322 τ_c), τ = 1.000 (= 1.296 τ_c τ = 0.780 (= 1.011 τ)$_{\dot{c}}$ and τ = 0.772 ($\sim$ τ)$_{\dot{c}}$

Figure 11(b). Spatial variations of ξ and e_{11} which are the solutions to eq.(4.28) under the boundary condition (4.27) at the same temperatures as those in Fig.12(a). Both ξ and e_{11} are normalized by $\bar{\xi}$ and $\bar{e}_{11}$, respectively. The embryo center x_0 is taken to be at origin.

Figure 11(c). Trajectories at the temperatures shown in Fig.12(a) are plotted on the contour maps of the potential surfaces. Those shown by open circles are representative points plotted at equal interval Δx of the coordinate x. Note that these trajectories pass through the saddle point on the potential surface.

Figure 12. Exact solutions to eq.(4.29) for various temperatures when $\kappa_2=0$. x_0 is taken to be at origin. (a) An embryonic fluctuation (eq.(4.31)) just above τ_c ($\tau=0.772\sim\tau_c$). (b) Antikink solution (eq.(B.2)) at the transition temperature. (c) Antikink solution (eq.(B.8)) below τ_c ($\tau=0.5=0.6479\tau_c$) representing the antiphase boundary separating two martensite variants. The

transformation scheme can easily be seen from these solutions (see also the Appendix B).

Figure 13. Relation between satellite reflections observed by Shapiro et.al.(Ref.) and the rhombohedral 'ghost lattice'. The arrows represent the directions of displacements from the exact commensurate cubic positions, whose relative magnitudes are expressed by the length of the arrows. Note that the satellites, with few exceptions, shift generally toward rhombohedral satellite positions (shown by open circles) while the fundamental Bragg reflections are centered on cubic reciprocal lattice points. (See also Fig.15.)

Figure 14. Rhombohedral 'ghost' reciprocal lattice when t soft mode is the zone boundary mode. Open and solid circles indicate superlattice and fundamental Bragg reflections, respectively. Note that only superlattice reflections have shifted while Bragg peaks do not shift, retaining the original cubic symmetry. The amount of the shifts of the satellite, shown by the arrows, are generally toward the rhombohedral commensurate satellite positions, i.e., the Bragg positions of the 'ghost lattice'.

Figure 15. Calculated diffraction patterns for $h \leq 4$, k=1 at the same temperatures as those in Fig.12. Notice the appreciable tailing (Huang scattering) of the fundamental Bragg peaks. The profiles of the satellites are shown in the insets with enlarged scales. The lines indicate the commensurate positions. It is

apparent that superlattice reflections are shifted, with their amount of shift increasing as |K| is increased, toward the origin of the reciprocal lattice while the Bragg peaks centered on the original reciprocal lattice points. Note that below $\tau<1$ satellites split into two peaks where the second peak seems to restore the commensurate positions.

Figure 16. Calculated 'ghost' behavior of the superlattice reflections at $\tau > \tau_c$. Large solid circles represent the fundamental Bragg reflections and small solid circles represent the superlattice reflections. The fundamental reflections always stay at the original regular positions (on the holizontal line), while superlattice reflections tend to shift to the commensurate positions of the low temperature lattice (shown by the open circles) as the temperature is lowered. Their actual positions are approximately half way between the commesurate positions of the high and the low temperature lattices.

Figure B.1. Schematic illustration of the ase transformation process. (a) Above τ_c embryonic fluctuations with different kind of variants are created randomly within the system. (b) The boundaries separating embryonic fluctuations from the matrix become kink-antikink pair. At the same time indirect interaction between these kinks develop by which the kinks can migrate. The kink-antikink pair of the same variant annihilate to form a large domain while an antiphase domain boundary is formed by a collapse of the kinks of the different variant. (c) Antiphase domain

boundaries would rearrange their positions due to the interaction between them. (d) Below τ_c martensite phase with a regular array of antiphase domains is formed.

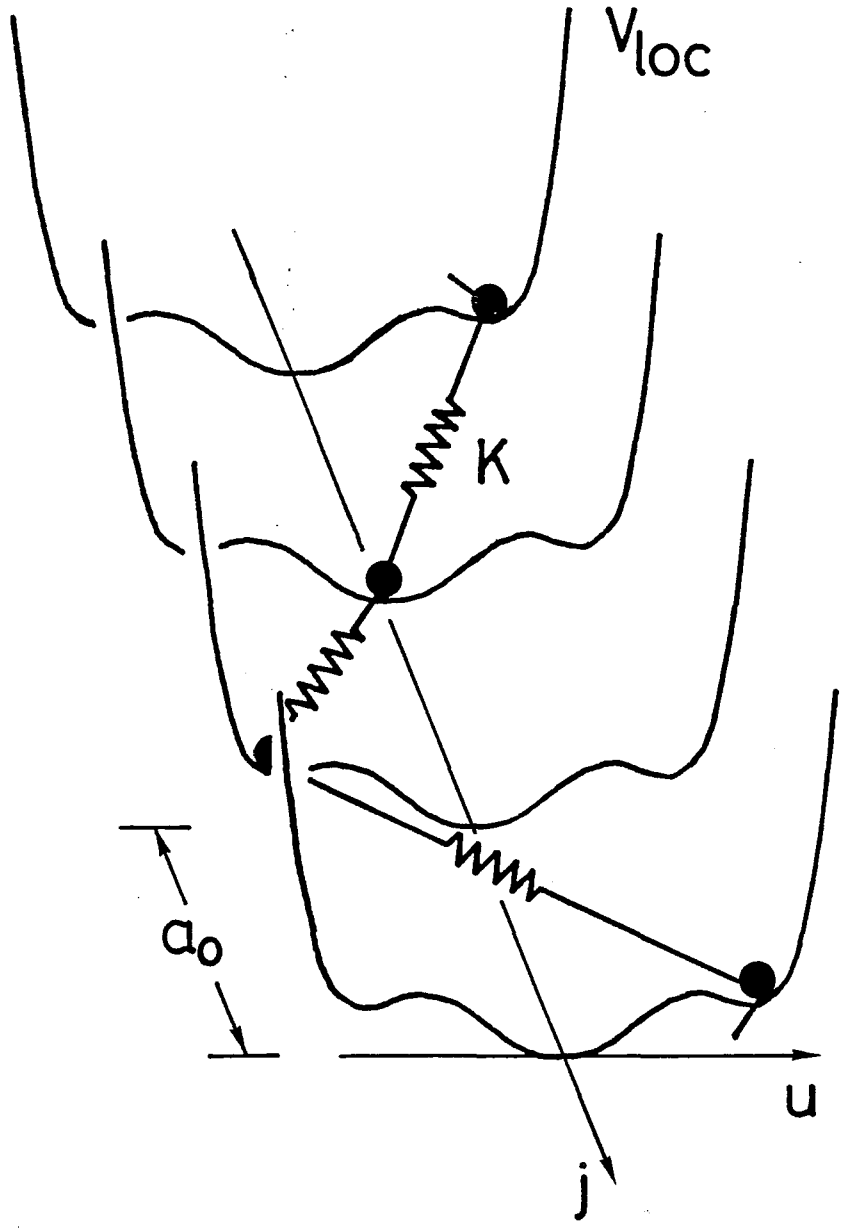

Fig. 1

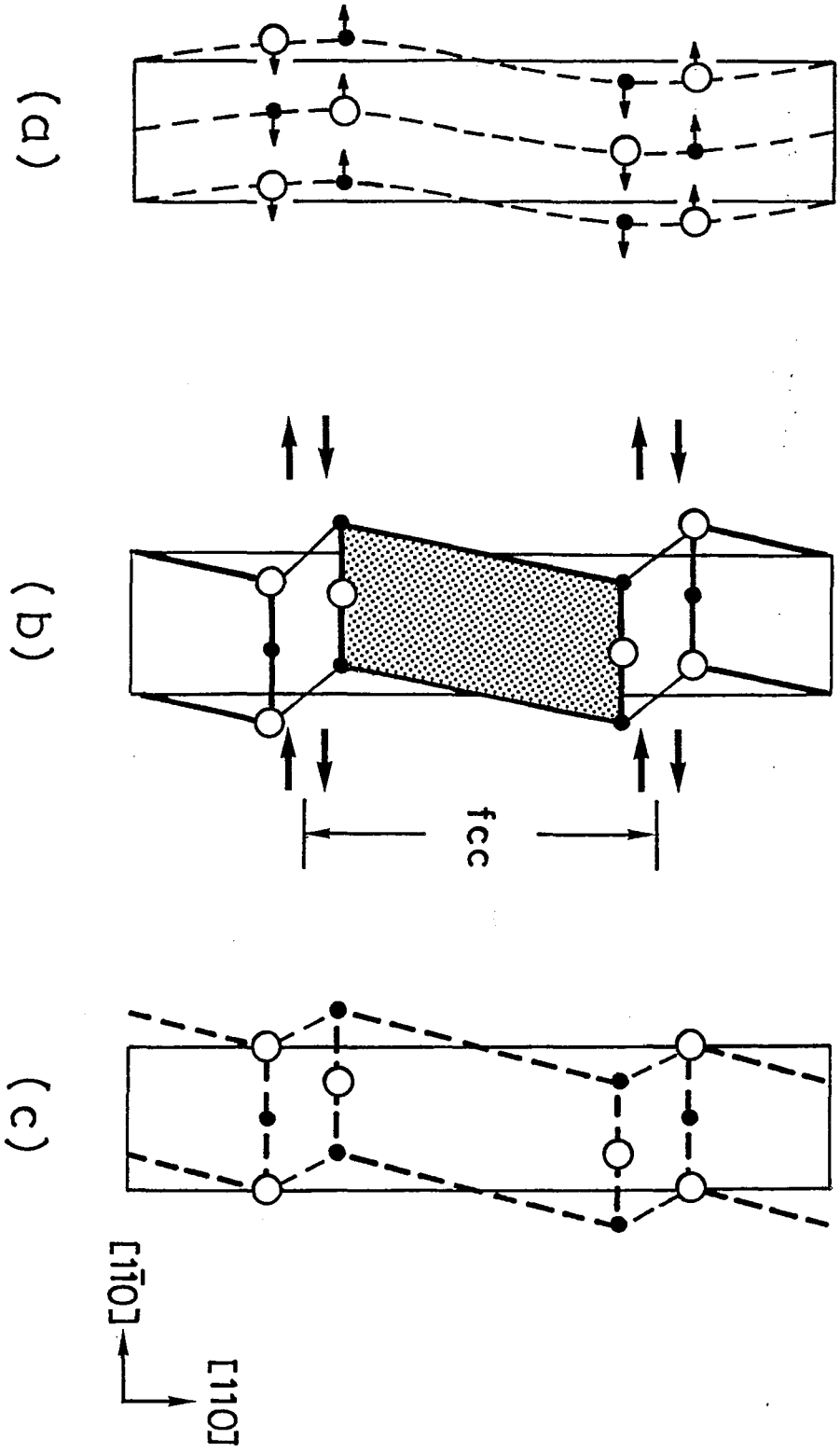

Fig. 2

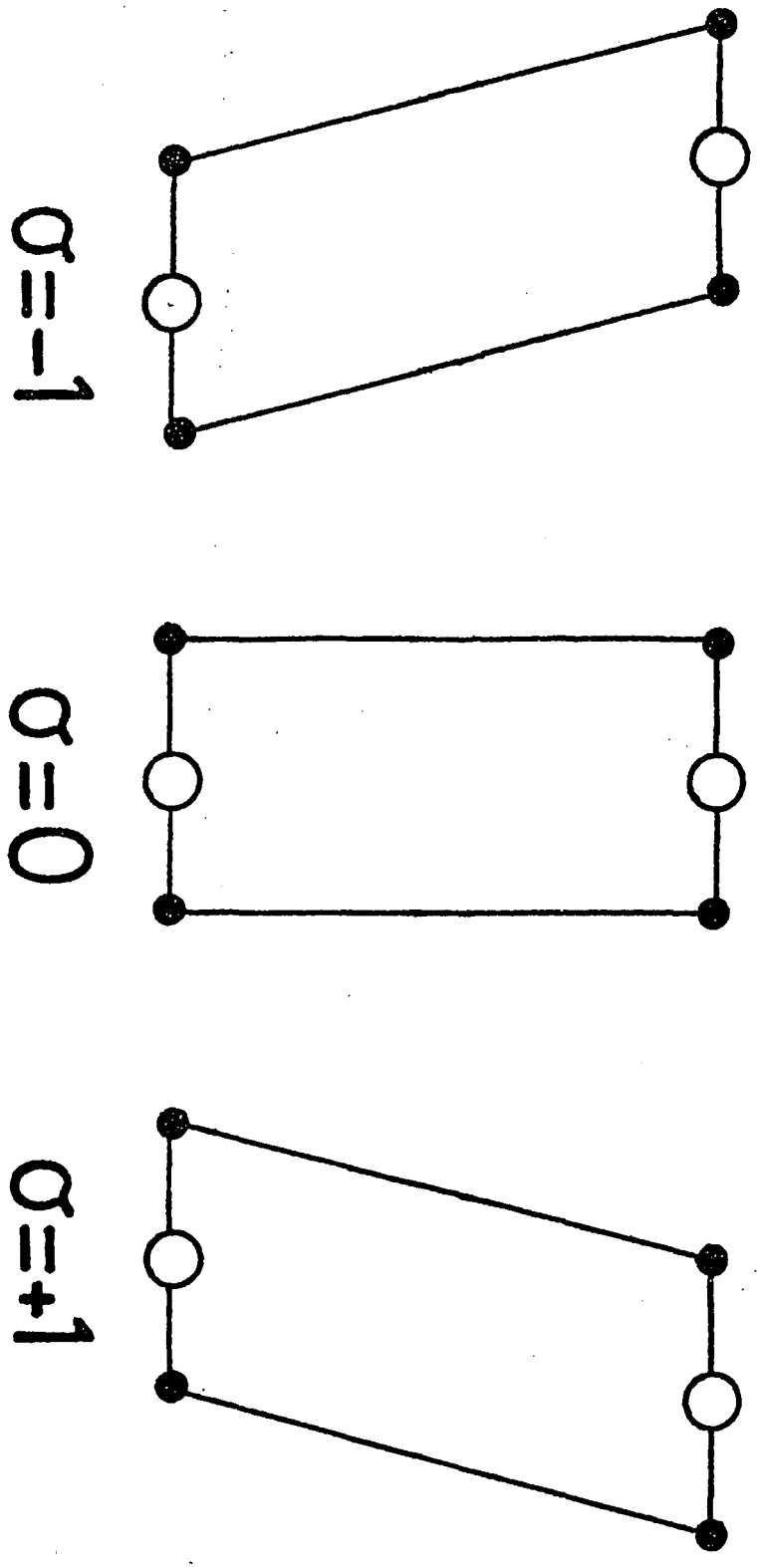

Fig. 3

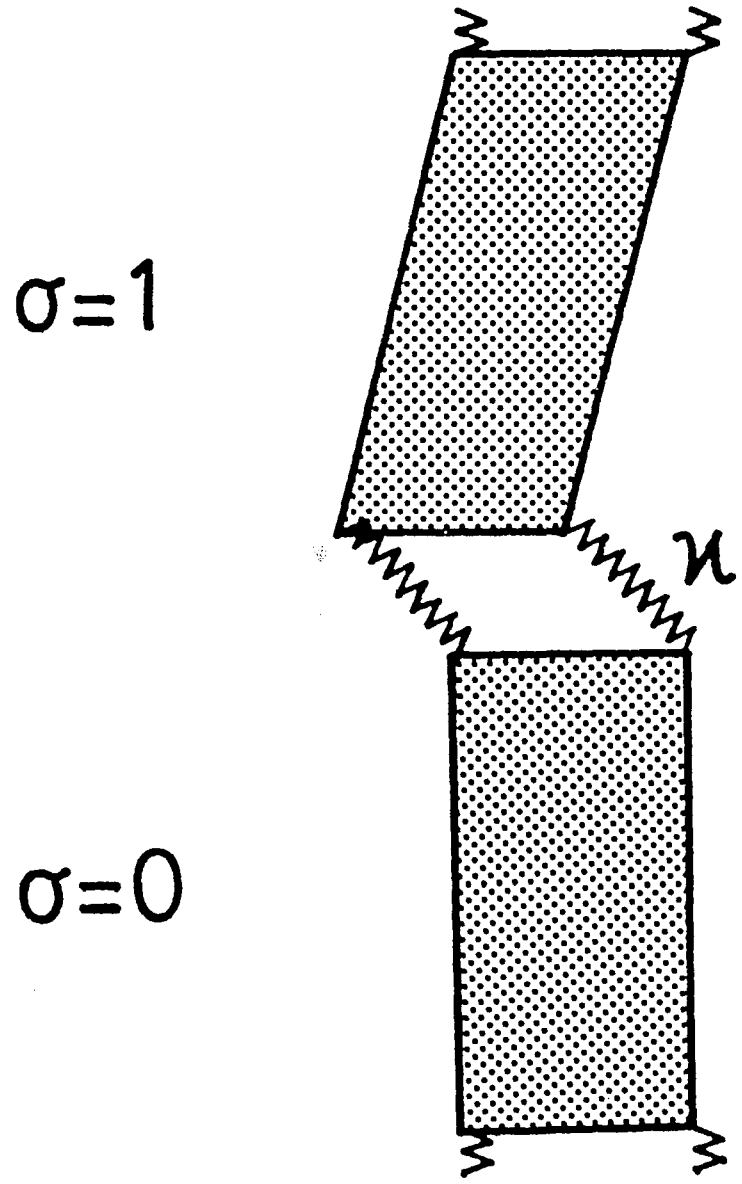

Fig. 4(a)

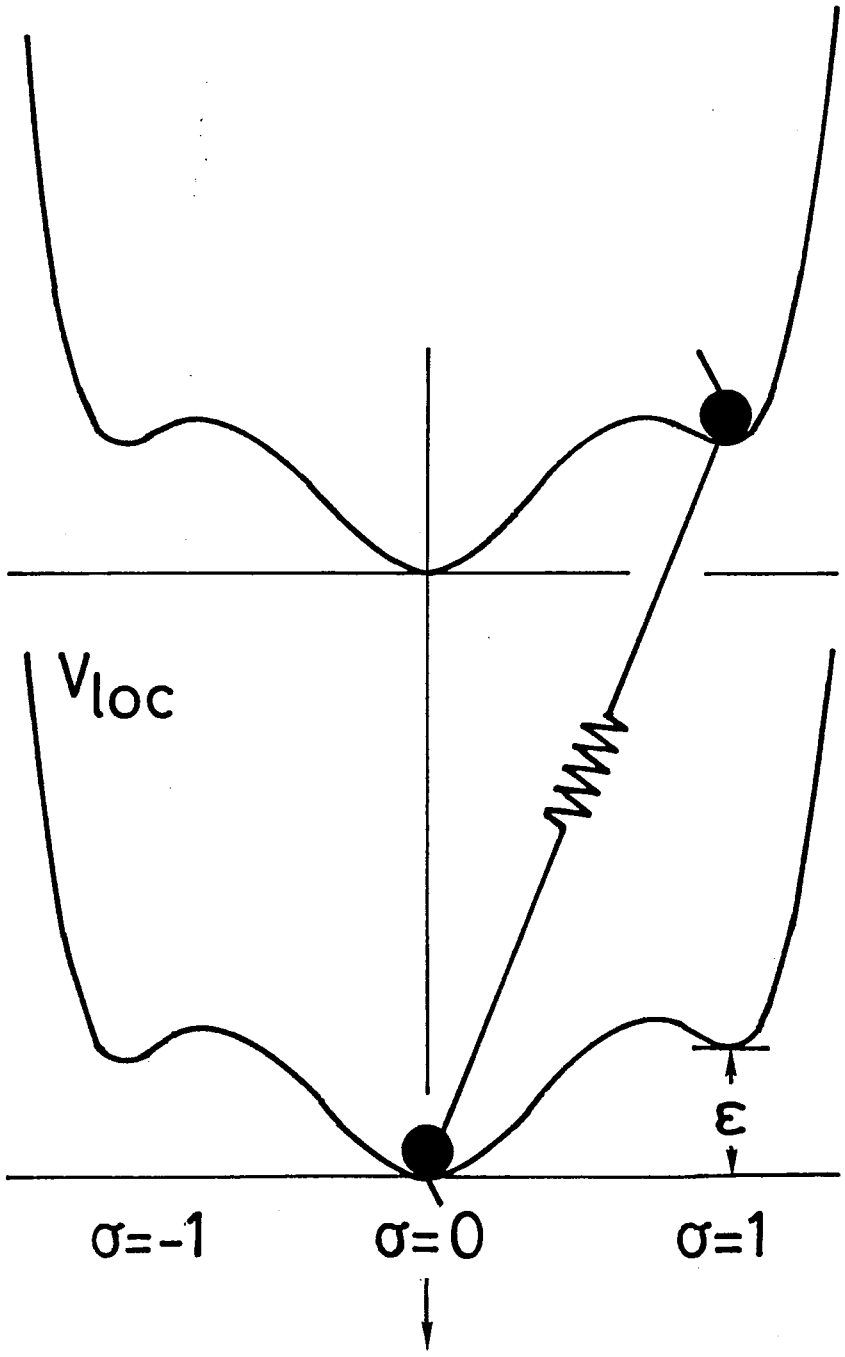

Fig. 4(b)

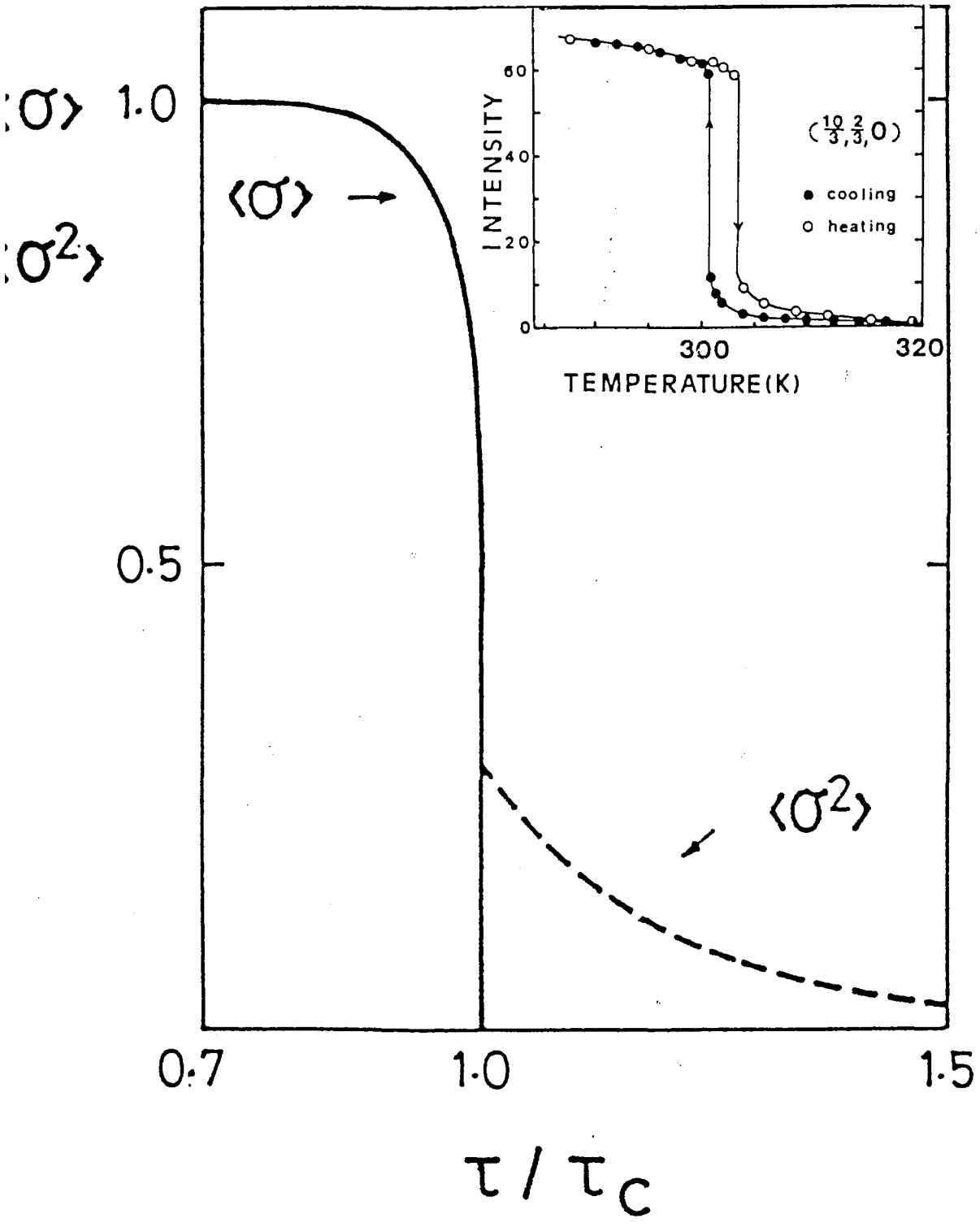
⟨σ⟩ 1.0
⟨σ²⟩
0.5
⟨σ⟩
⟨σ²⟩
0.7
1.0
1.5
τ / τc
INTENSITY
60
40
20
0
300
320
TEMPERATURE(K)
(10/3, 2/3, 0)
cooling
heating

Fig. 5

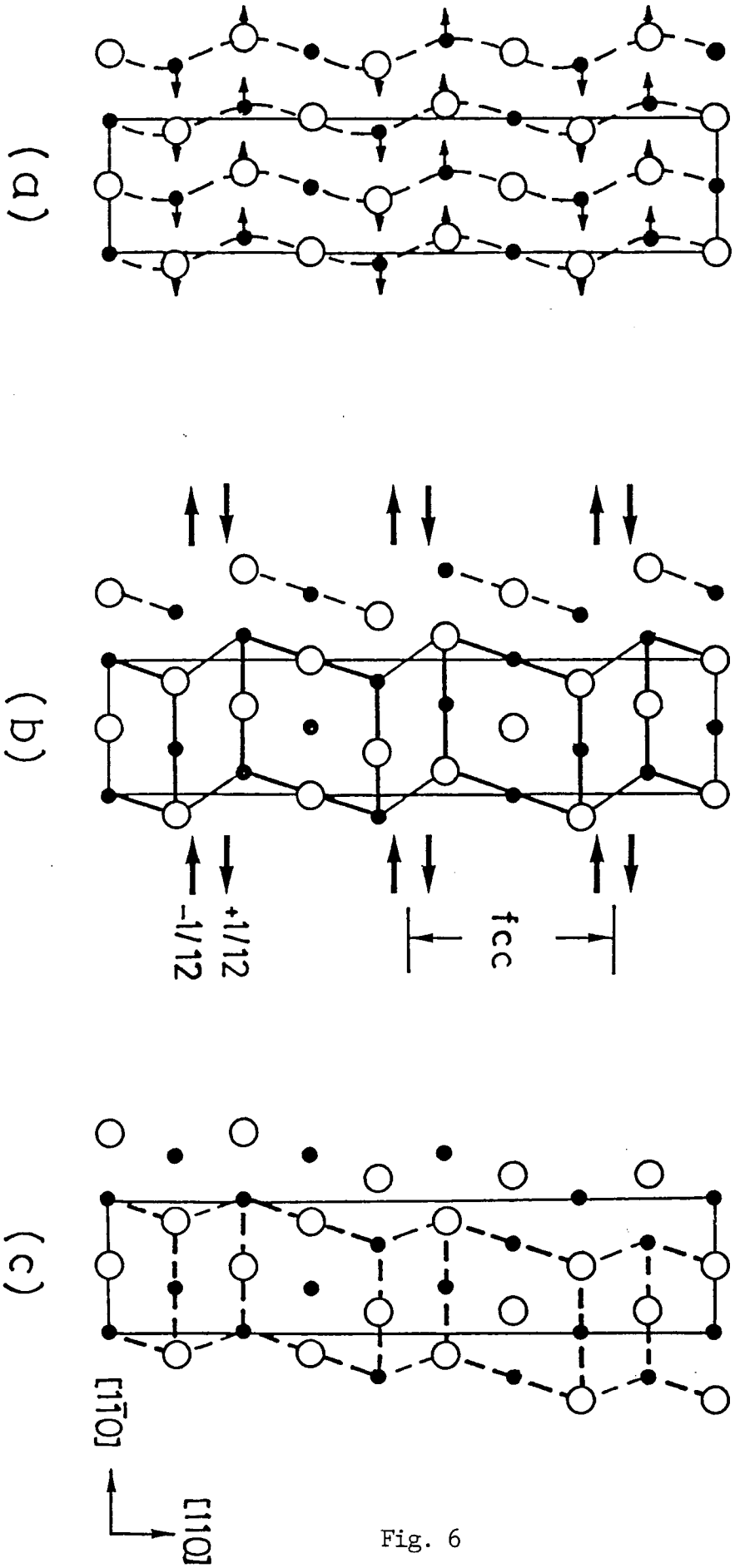

Fig. 6

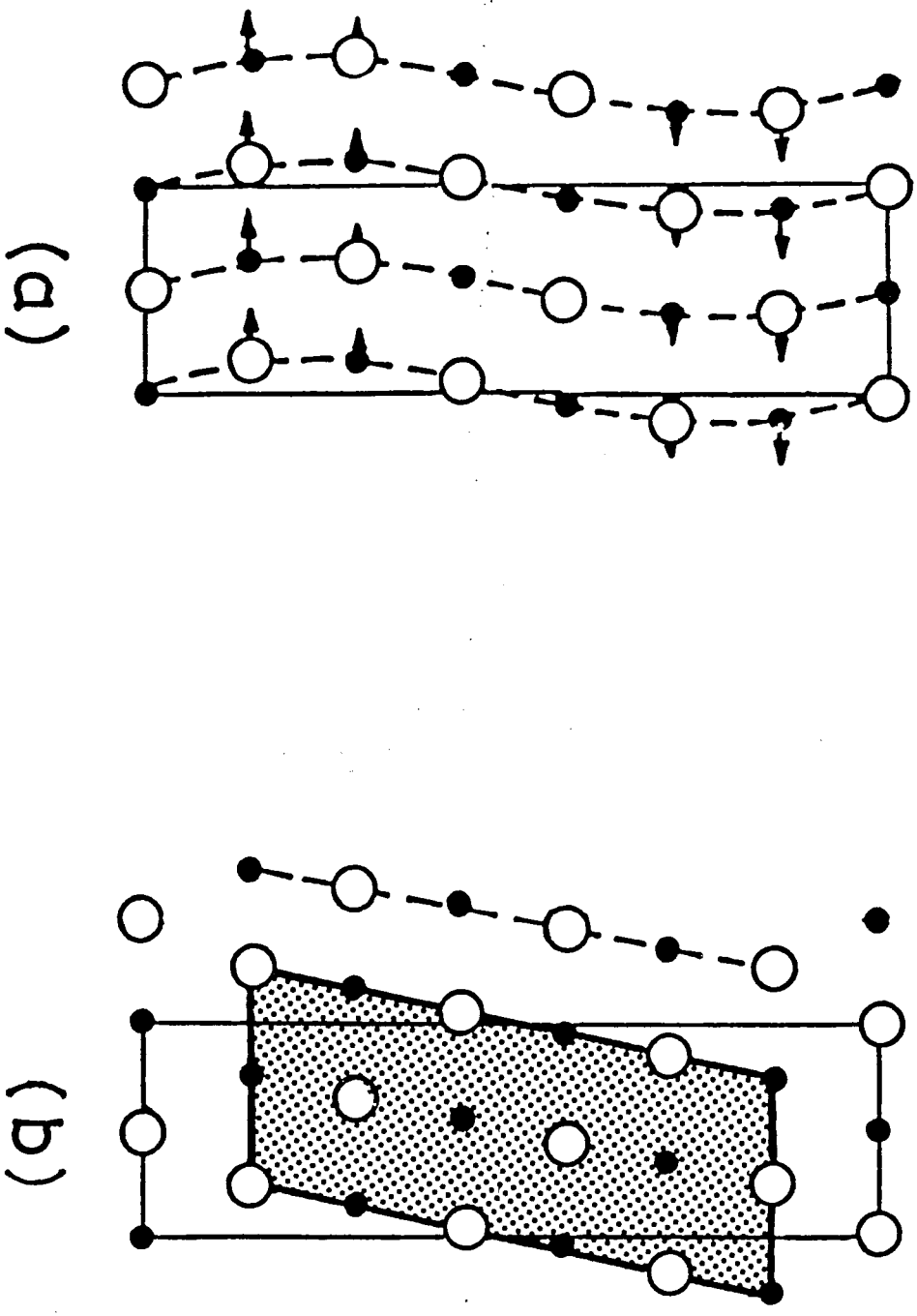

Fig. 7

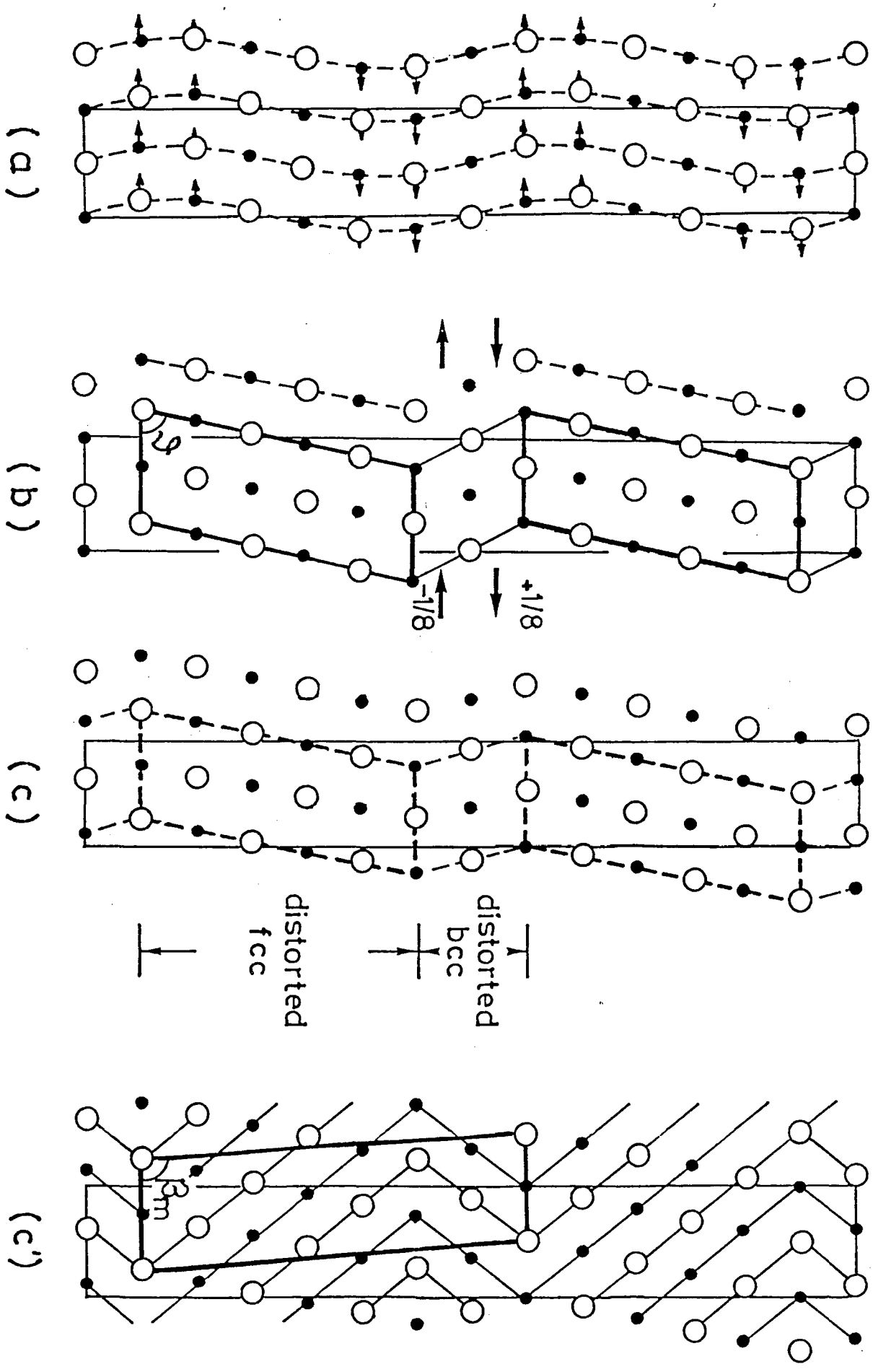

Fig. 8

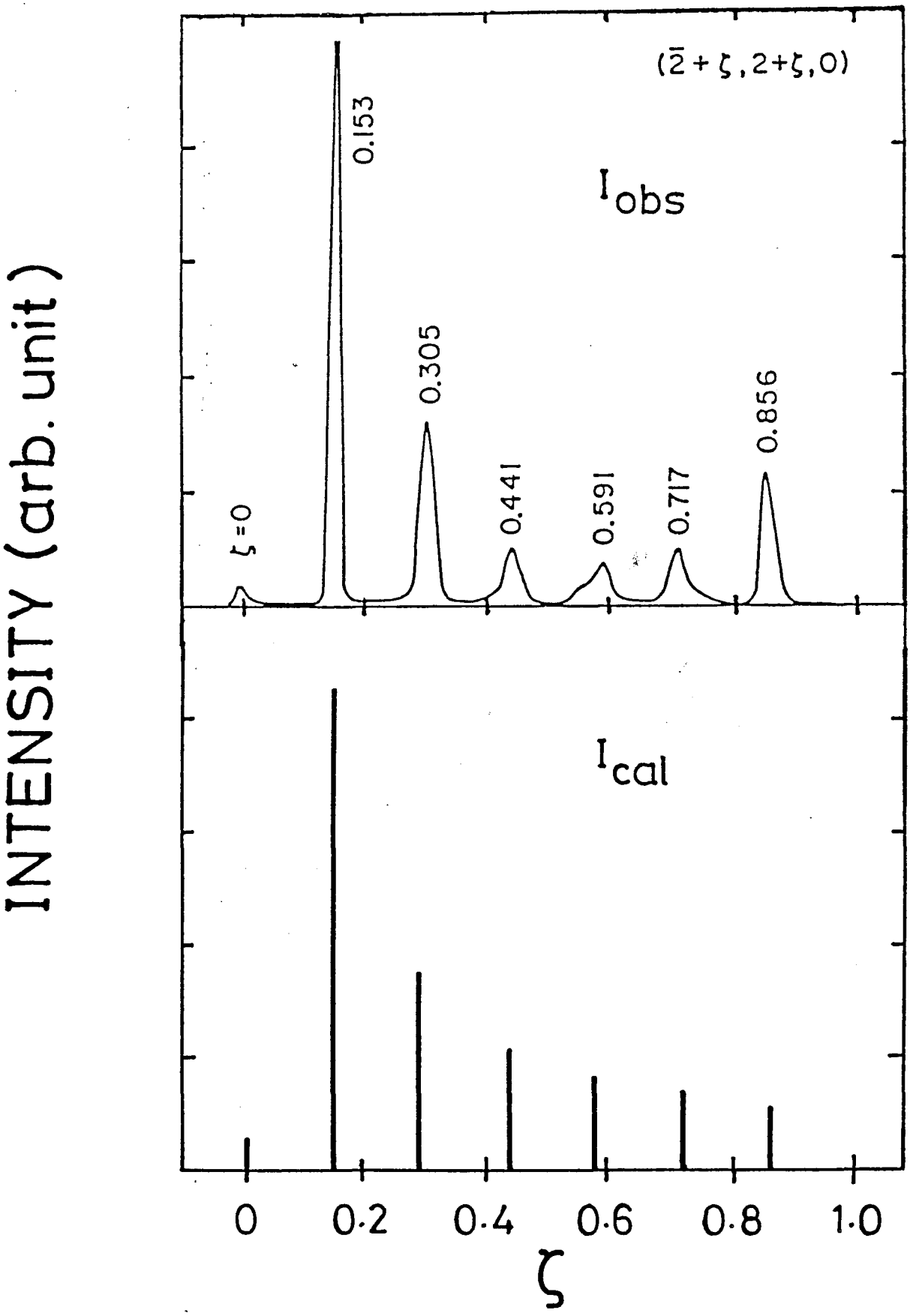
INTENSITY (arb. unit)
$(\bar{2}+\zeta, 2+\zeta, 0)$
I_{obs}
I_{cal}
ζ=0
0.153
0.305
0.441
0.591
0.717
0.856
0
0·2
0·4
0·6
0·8
1·0
ζ

Fig. 9

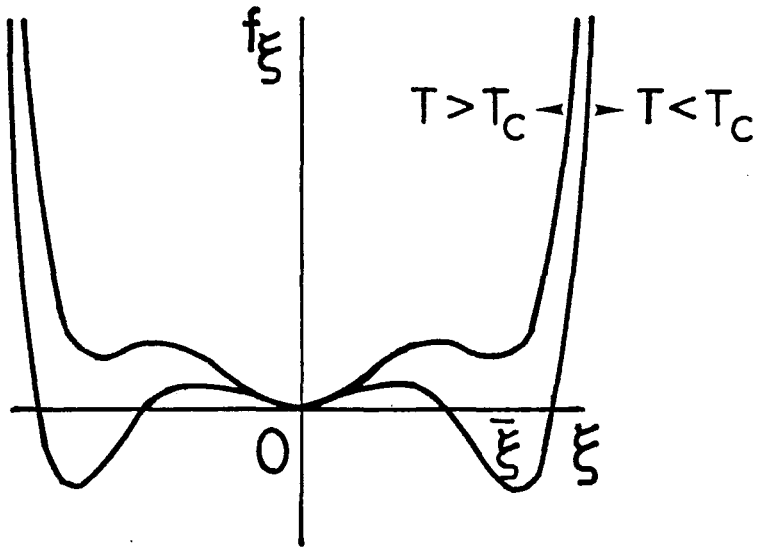

Fig.10

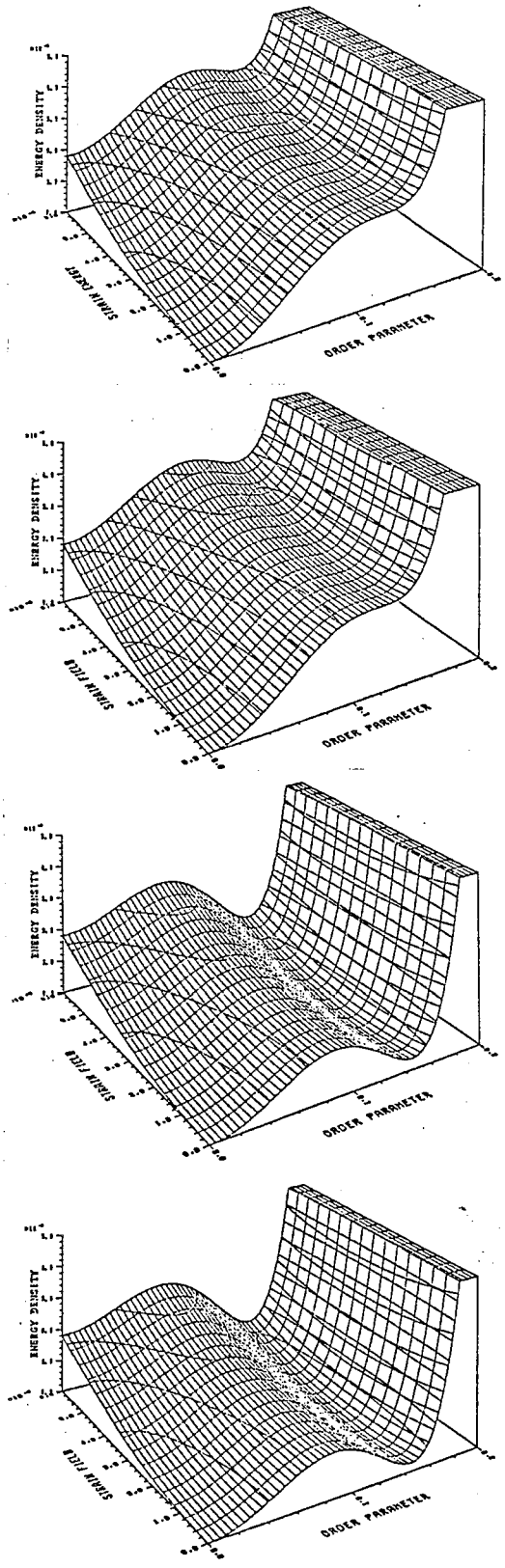
ENERGY DENSITY
SIMAN FIELD
ORDER PARAMETER
τ=1.322τc
τ=1.296τc
τ=1.011τc
τ~τc

Fig.11(a)

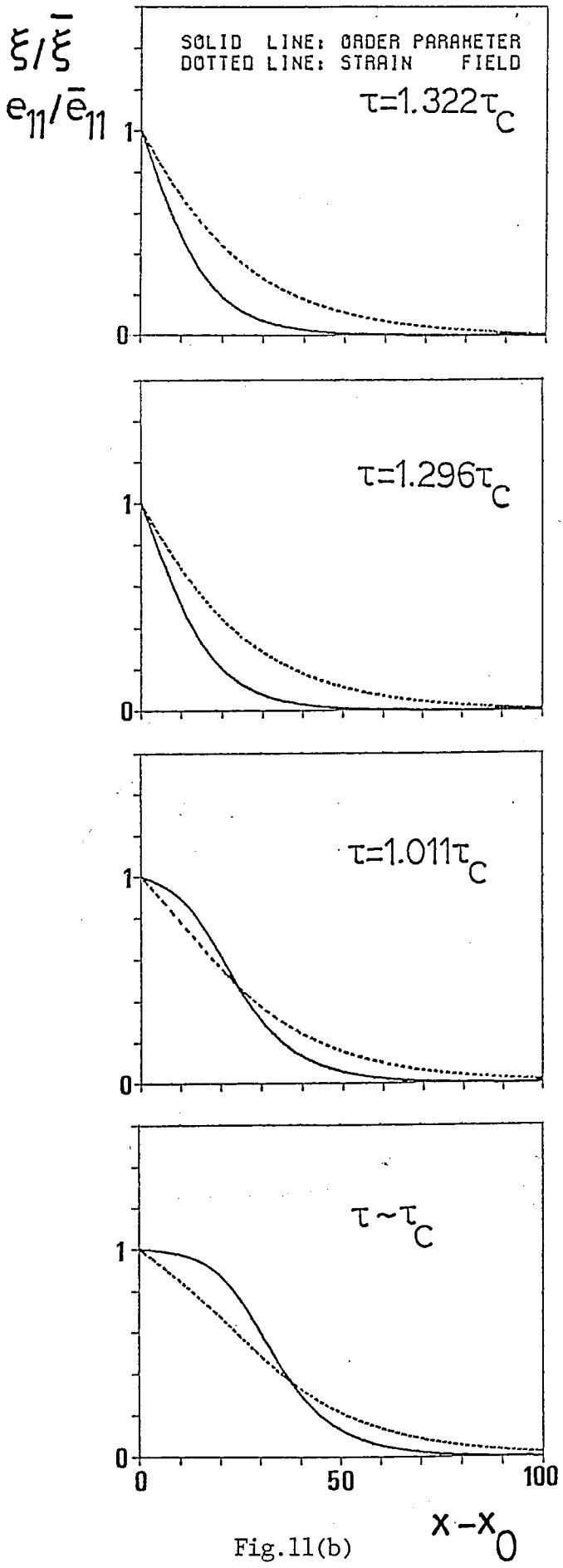
ξ/ξ̄
e11/ē11
SOLID LINE: ORDER PARAMETER
DOTTED LINE: STRAIN FIELD
τ=1.322τc
τ=1.296τc
τ=1.011τc
τ~τc
1
0
0
50
100
x-x0

Fig.11(b)

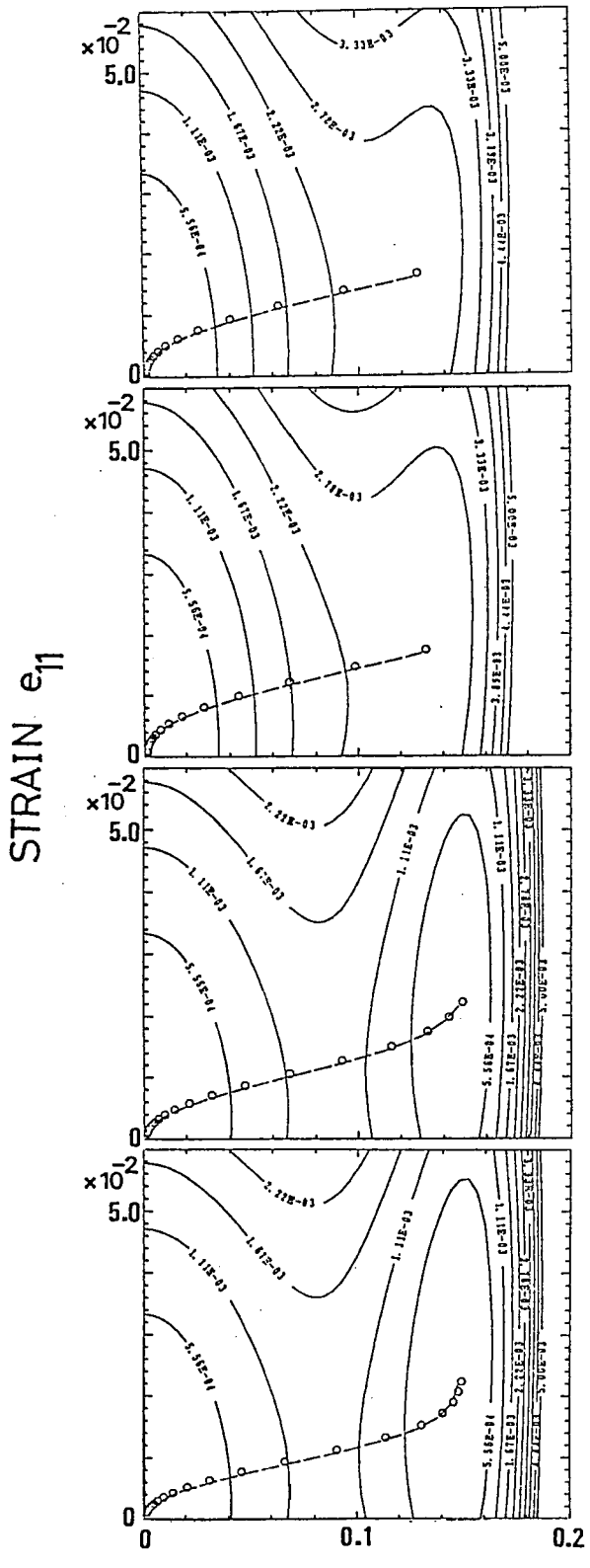
τ=1.322τc
τ=1.296τc
τ=1.011τc
τ~τc
STRAIN e11
ORDER PARAMETER ξ
×10-2
5.0
0
0.1
0.2

Fig.11(c)

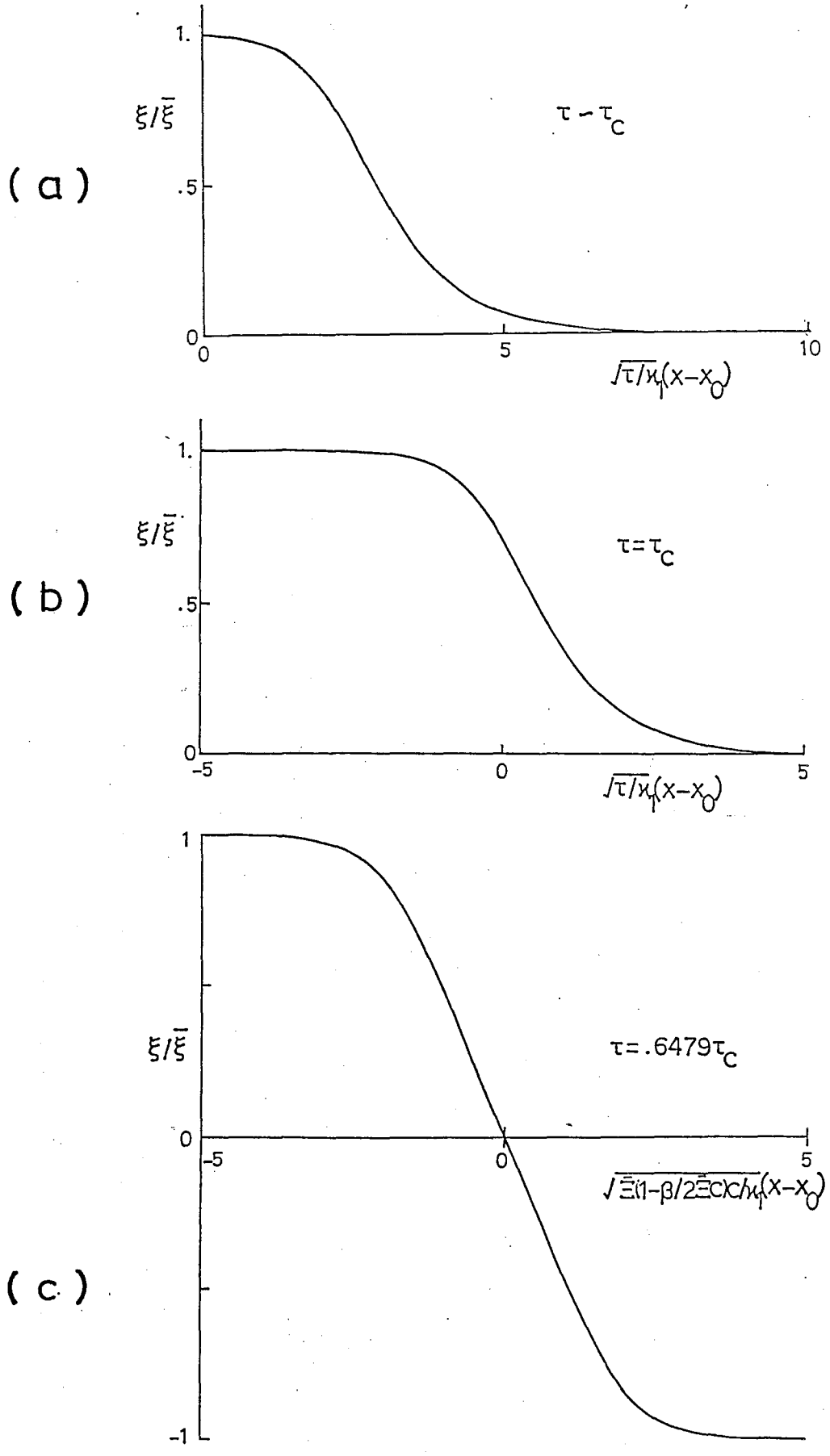
(a)
1.
.5
0
ξ/ξ̄
0
5
10
τ - τc
√τ/κ1(x-x0)
(b)
1.
.5
0
ξ/ξ̄
-5
0
5
τ=τc
√τ/κ1(x-x0)
(c)
1
0
-1
ξ/ξ̄
-5
0
5
τ=.6479τc
√Ξ(1-β/2Ξc)c/κ1(x-x0)

Fig.12

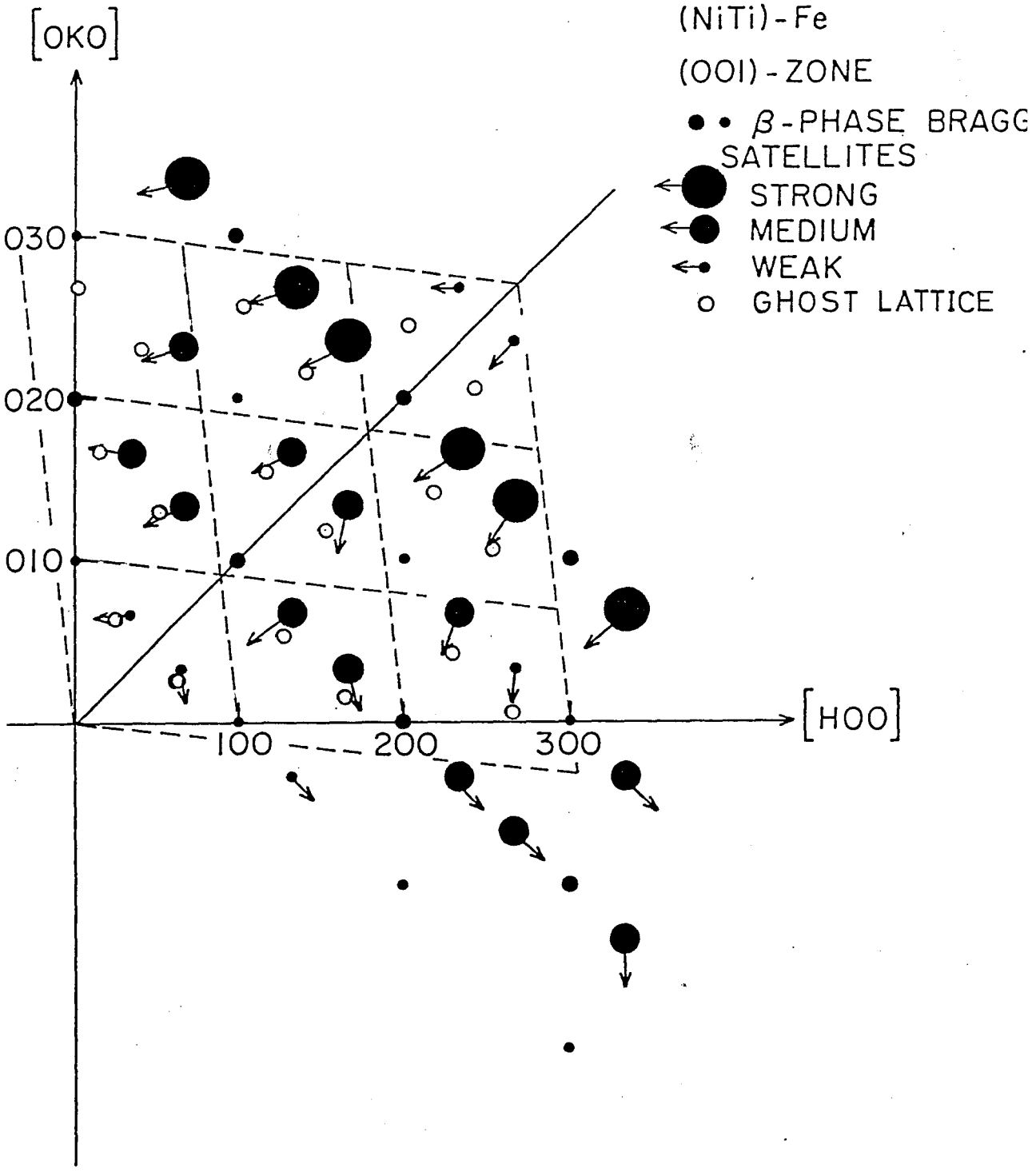
[OKO]
030
020
010
100
200
300
[HOO]
(NiTi)-Fe
(OOI)-ZONE
β-PHASE BRAGG SATELLITES
STRONG
MEDIUM
WEAK
GHOST LATTICE

Fig.13

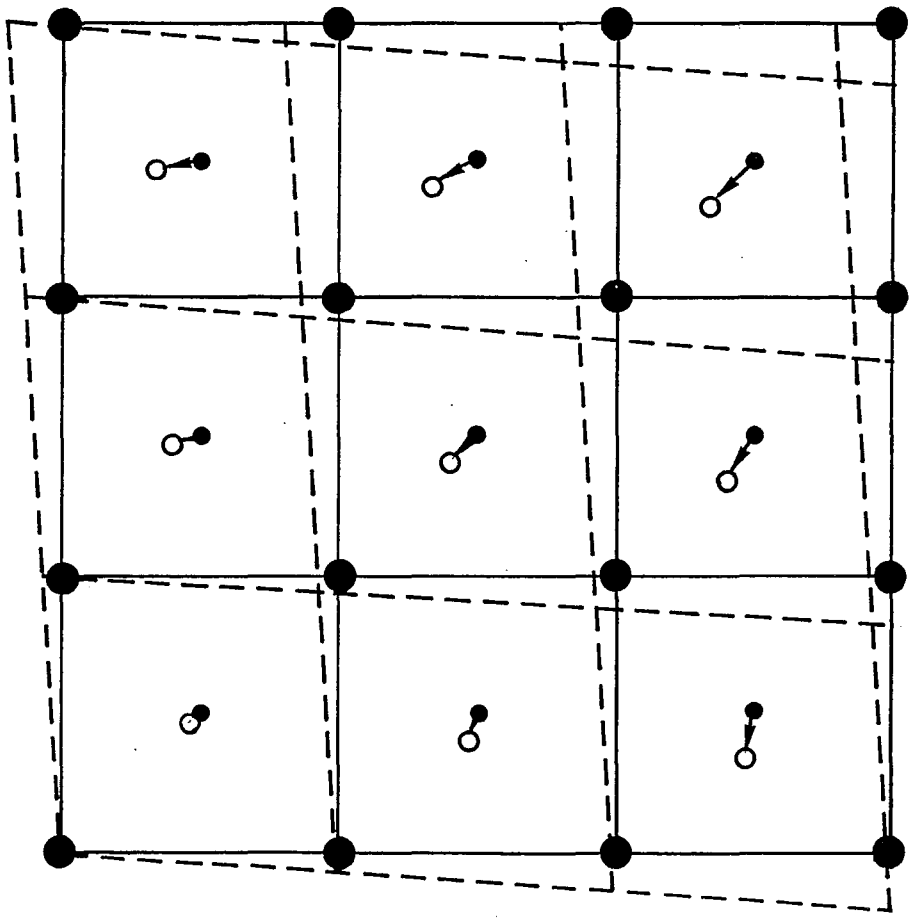

Fig.14

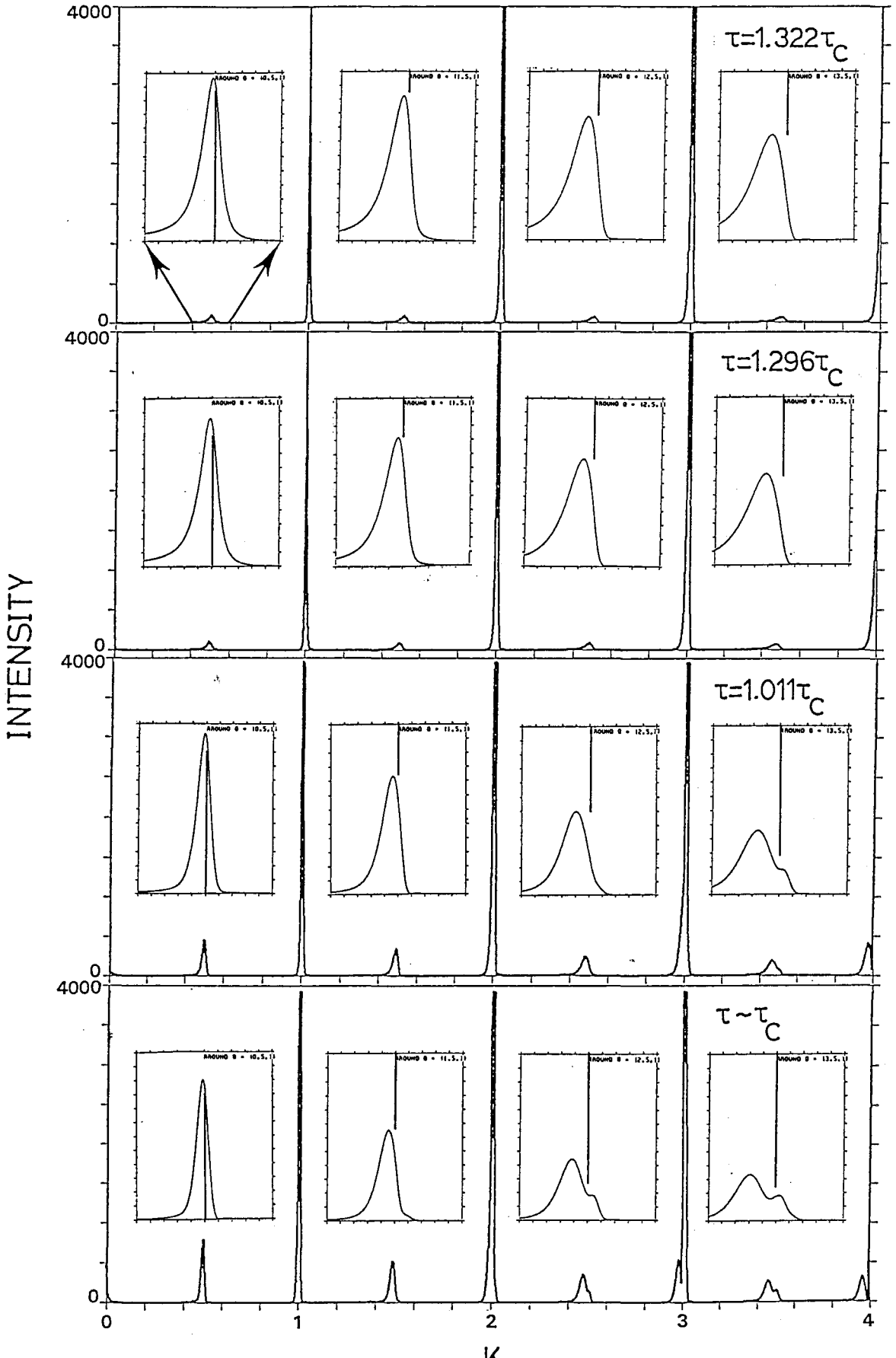

Fig.15

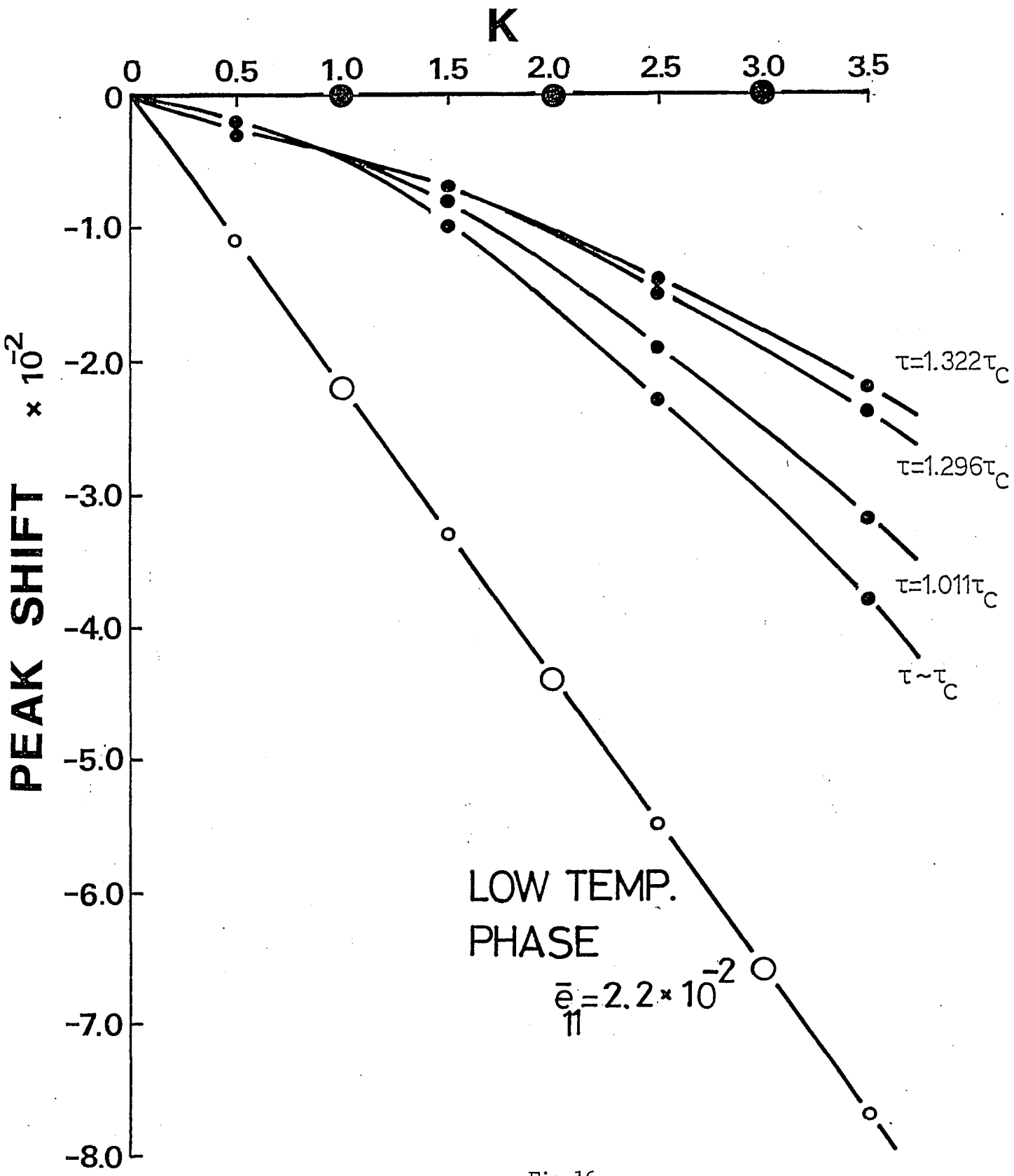
K
0
0.5
1.0
1.5
2.0
2.5
3.0
3.5
PEAK SHIFT × 10^-2
0
-1.0
-2.0
-3.0
-4.0
-5.0
-6.0
-7.0
-8.0
τ=1.322τc
τ=1.296τc
τ=1.011τc
τ~τc
LOW TEMP.
PHASE
ē11=2.2×10^-2

Fig.16

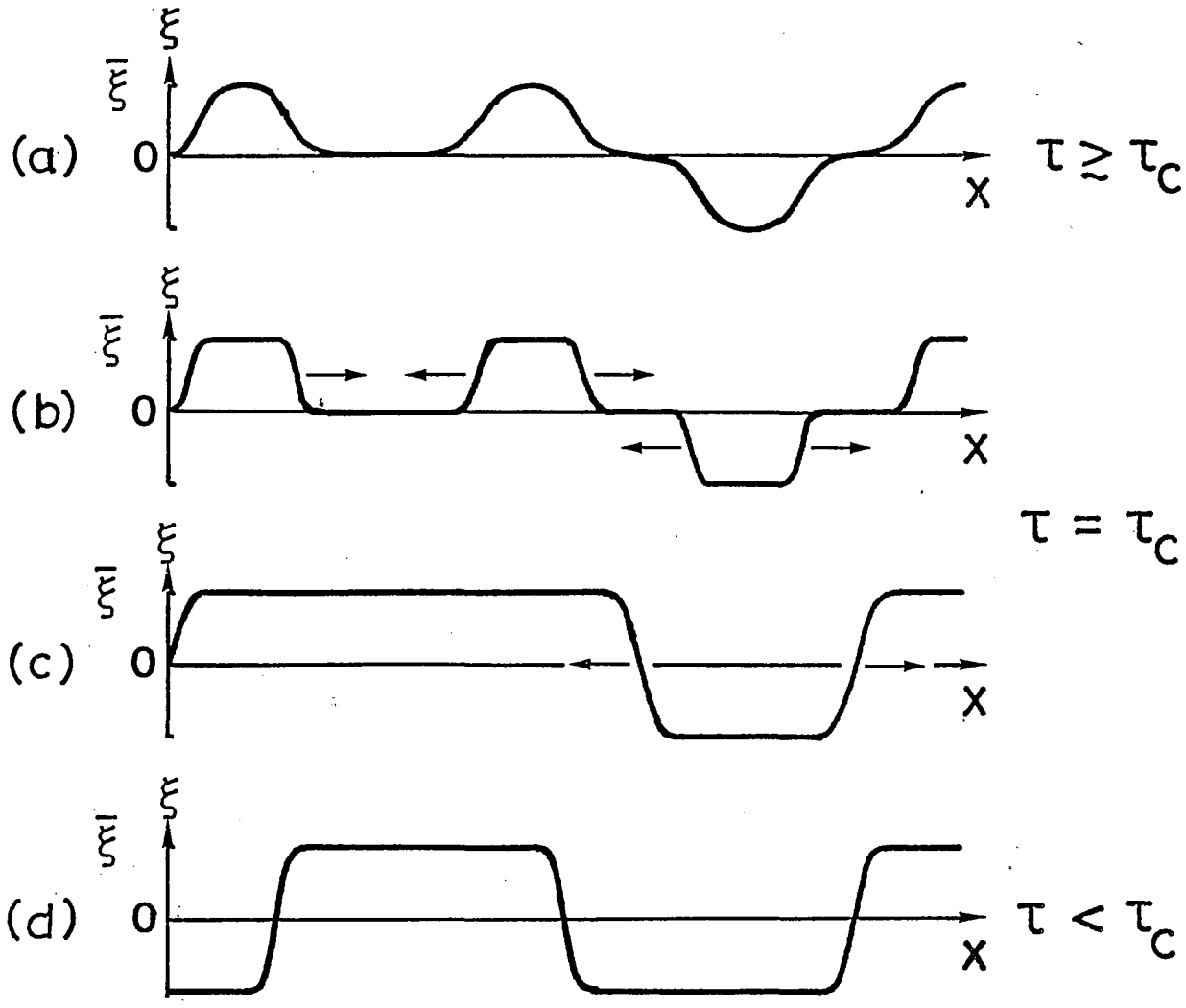

Fig. B. 1